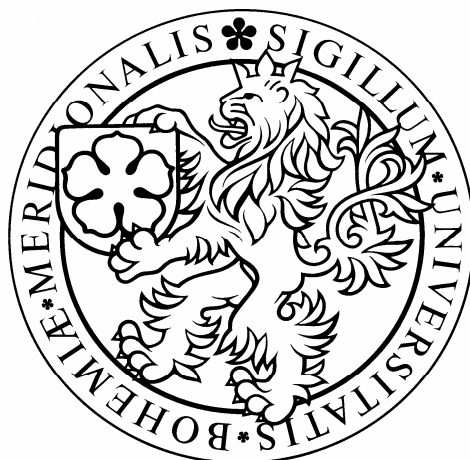Faculty of Science of the University of South Bohemia

Miroslav Kloz

Energy transfer pathways in reconstituted peridinin chlorophyll complexes

Master thesis

Supervisor: Prof. RNDr. Tomáš Polívka, PhD.

České Budějovice 2009

Annotation: : The main objective of this thesis is to study energy transfer pathways between carotenoids and chlorophylls in the reconstituted light harvesting protein, peridinin chlorophyll protein (PCP), of the marine dinoflagellate *Amphidinium carterae*. The reconstituted PCP complex contains either bacteriochlorophyll-a or a mixture of bacteriochlorophyll-a and chlorophyll-b instead of chlorophyll-a that occurs in the native PCP. The introduction and methods of the thesis describes spectroscopic properties of carotenoids with emphasis on the carotenoid peridinin, and a brief introduction to the femtosecond pump probe spectroscopy and global fitting analysis used for treating the time resolved spectra. The main results, dependence of the peridinin to bacteriochlorophyll-a energy transfer pathways on excitation wavelength and energy transfer between chlorophylls, are described and discussed in the results of the thesis.

Prohlašuji, že svoji diplomovou práci jsem vypracoval samostatně pouze s použitím pramenů a literatury uvedené v seznamu citované literatury.

Prohlašuji, že v souladu s § 47b zákona č.111/1998 SB. v platném znění souhlasím se zveřejněním své diplomové práce, a to v nezkrácené podobě elektronickou cestou ve veřejně přístupné části databáze STAG provozované Jihočeskou univerzitou v Českých Budějovicích a na jejích internetových stránkách.

5. Ledna 2009

Podpis:

Acknowledgment:

Contents

List of abbreviations:

PCP   peridinin-chlorophyll protein
τ lifetime of excited state
S1   excited state of carotenoids (1.1)
S2   excited state of carotenoids (1.1)
~   approximately equal
Å   Ångström (10^{-10} m)
[num.]   reference in text, physical unit in graphs
(num.)   reference to the other chapter
Chl   chlorophyll
Chl-a   chlorophyll a
Chl-b   chlorophyll b
Bchl-a   bacteriochlorophyll a
Δ increment of physical quantity
E   energy
t, t time
±value   95% trust region
k   magnitude of wave vector
ν wavenumber in cm^{-1}
λ wavelength
IR   infrared spectral region
DS   difference spectra
EADS   evolution associated difference spectra
RDS   relative degradation spectra
st.st.   steady state
ex.   excitation
h Plank constant 6.626 . 10^{-34} J.s
μ dipole moment of molecule
ε extinction coefficient
Γ half width
κ orientation factor
n refractive index
l spatial distance
c speed of light in vacuum
NMR   nuclear magnetic resonance

1. Introduction:

Photosynthetic pigments play a crucial role in the mechanisms of photosynthesis. They act not only in reaction centres, but also in the so-called light harvesting antennas. Reaction centres perform the central process of primary photosynthesis, which is the charge separation and stabilization. They use for the process energy captured from light. But reaction centres would stay inactive for most of the time under standard light conditions on the Earth, because of a small effective cross-section of the chlorophyll molecule. It is not a principal problem and organisms could solve it by synthesizing a sufficient number of reaction centres to provide all needful energy, but photosynthetic organisms found a different solution. Instead of synthesizing a large number of spare reaction centres, they connect reaction centres with light harvesting antennas.
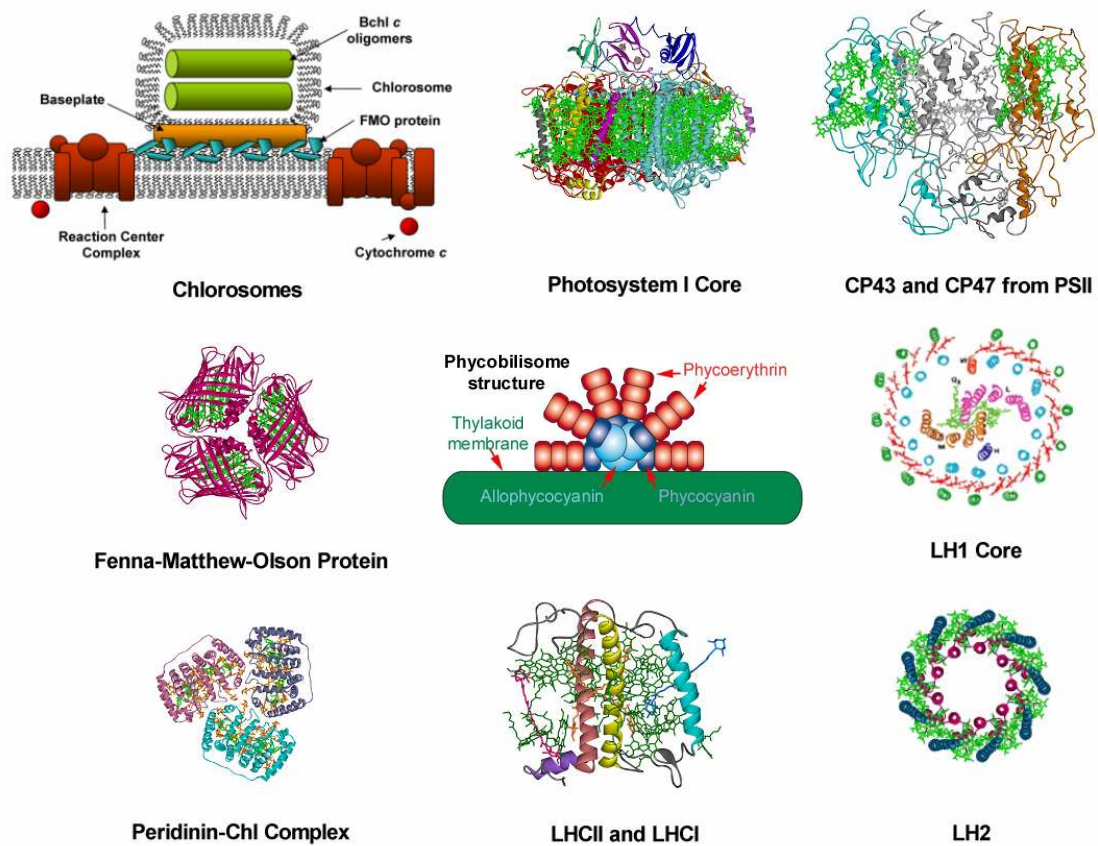

Fig.: 1 Structures of selected light harvesting antenna complexes occurring in nature.

These antennas maintain sufficient flux of energy when the light intensity is too low to propel reaction centres effectively, and on the other hand, some antennas contains a

photoprotective machinery that protects the photosynthetic apparatus from the over-excitation under high-light conditions [1]. While the pigments composition and architecture of reaction centres is very uniform among the photosynthetic organisms, the antennas display a very broad variety of pigment compositions and structures (Fig.: 1). This enables photosynthetic organisms to inhabit biotopes with very different conditions of both light intensity and spectrum. To successfully manage the spectral variation of light in various habitats, organisms employ in their light harvesting systems besides chlorophylls also many different carotenoids [2]. In some organisms, carotenoids even become the main light harvesting pigments. This is a case of peridinin chlorophyll-a complex (PCP) [3], which is a subject of this thesis and will be treated in a detail in a separate chapter (1.3).

Since the main task of antenna complexes in all organisms is to absorb light and funnel it, via a cascade of pigments, into the reaction centre, the key process enabling antenna to fulfil this task is excitation energy transfer between the pigments within the antenna complex. The energy transfer may occur by various mechanisms, ranging from a trivial case of radiative transitions to a set of non-radiative processes including excitonic coupling between pigments, Dexter electron exchange mechanism, and Förster dipole (or other multipole) interaction. In many antenna systems two or even more of these processes act together in dependence on the distance and mutual position of individual pigments.

A radiative energy transfer is a process where a photon is emitted by a donor molecule and absorbed by an acceptor molecule. These processes can take place on an almost arbitrary distances and their duration depends on the lifetime of an excited state of the emitting molecule that is for chlorophylls usually on a nanosecond timescale. This type of energy transfer is of negligible importance in photosynthetic light-harvesting systems.

The Förster type of coupling is based on a dipole-dipole interaction where the dipoles of involved molecules act together in an analogy with coupled pendulums in classical mechanics. This process takes place on larger distances, usually up to 100 Å. The magnitude of the Förster coupling drops with the sixth power of distance similar to the van der Waals interaction (intensity of Förster type interaction ~ $1/R^6$). An example is energy transfer between Bchl-a in the B800 ring in purple bacterial LH2 antenna (Fig. 1).

The Dexter type of the energy transfer is a process where wave functions of the pigments overlap to a certain extent allowing an electron exchange. This process takes place usually on a very short distances (below 10 Å) and its magnitude drops exponentially with the distance (intensity of Dexter type interaction ~ exp(-R)). The Dexter interaction is typical (but not restricted) of triplet-triplet transitions. Since the Dexter-type coupling does not depend on magnitude of dipole moments, the Dexter mechanism can be also active in energy transfer involving forbidden states having negligible dipole moments preventing Förster-type coupling.

The excitonic coupling takes place when the pigments are in such a close contact, that their electronic wave functions merge together to form one complex sharing the excitation in a form of a virtual particle called exciton. In this case, a whole bunch of pigments is always excited simultaneously, and it is not possible to talk about excitation of individual pigments inside the bunch. Characteristic examples of the excitonic coupling are chlorosomes (Fig. 1) or B850 and B875 rings of LH2 and LH1 antenna complexes of purple bacteria, in which Bchl molecules are tightly packed.

On the basis of the known structures of various antenna complexes (Fig. 1) and knowledge of dipole moments of various photosynthetic pigments, it is possible to estimate that individual energy transfer steps occurring via the energy transfer mechanisms briefly described above occur on time scales ranging from hundreds of femtoseconds to hundreds of picoseconds. Consequently, to follow these processes it is required to employ techniques working with a sub-picosecond time resolution. Since 1980's spectroscopic methods using lasers with sub-picosecond pulses have been established. Nowadays, time-resolved spectroscopy with sub-100 fs resolution has become a standard for studies of various ultrafast processes in both natural and synthetic systems. With these methods we are now able to track paths of the energy transfer within light harvesting complexes. Brief introduction to the time-resolved spectroscopic methods with emphasis on those used in this thesis is presented in the Chapter Methods (2.).

1.1 Excited states of carotenoids

Carotenoids are a large group of pigments occurring in nature. Currently, more than 1000 different carotenoids have been identified, fulfilling various functions in biological

systems, ranging from anti-oxidative properties to photo-protection and light-harvesting. All carotenoids share a common structural motif; a backbone consisting of alternating single and double bonds that form a conjugated π-electron system responsible for most of the spectroscopic properties of carotenoids. Most carotenoids occurring in organisms have a backbone consisting of 7 to 13 double bonds while the structures at the ends of the backbone vary significantly among the individual carotenoids. For the majority of carotenoids, their conjugated system can be approximated by the C_{2h} symmetry group. In terms of symmetry labels of the C_{2h} point group, carotenoids have two main singlet exited states. The $2^1A_g^-$ state that is the lowest excited state and is usually called the S_1 state, and the $1^1B_u^+$ state that is, due to historical reasons, usually called the S_2 state. The transition from the ground (S_0) state to the S_1 state is symmetry forbidden because the S_0 state has the A_g^- symmetry [2], while the S_0-S_2 transition is allowed. Experiments together with calculations set the forbidden S_1 state to be lower than the S_2 state for all carotenoids occurring in nature [2].

The S_0-S_2 transition causes the dominant structures in the absorption spectrum of carotenoids (Fig. 2). It is characterised by a wide absorption band usually situated between 350 and 550 nm, in which three to four peaks assigned to the lowest vibrational levels are distinguishable. The decreasing temperature makes the vibronic transitions more pronounced. The S_2 state energy increases with the decreasing of the length of the backbone (similar to the energy of the "particle in a box" model) ranging from 19 000 cm^{-1} (526 nm) for spirilloxanthin with conjugation length N=13 to 20 960 cm^{-1} (477 nm) for fucoxanthin with N=7. Both these values refer to CS_2 as a solvent [23], because energy of the S_2 state also depends both on the polarizability and polarity of the solvent. In a highly polarizable environment (such as in CS_2), the S_2 state is usually red shifted in a range of tenths of nm [24]. Effects of polarity are strong for the carotenoids possessing a conjugated carbonyl group (e.g. peridinin), but become negligible for other carotenoids. In case of carbonyl-containing carotenoids in polar solvents, the absorption spectrum is usually asymmetrically broadened towards longer wavelengths and the vibrational structure of the S_0-S_2 transition is lost. It was suggested that this effect is mostly due to the charge transfer character of the ground state that induces broader conformational disorder [25]. Similar effects on the S_0-S_2 transition are observed in protic solvents, and they were hypothesized to be responsible for creating a hydrogen bond with carbonyl oxygen, thus further stabilizing the charge transfer character of the ground state.
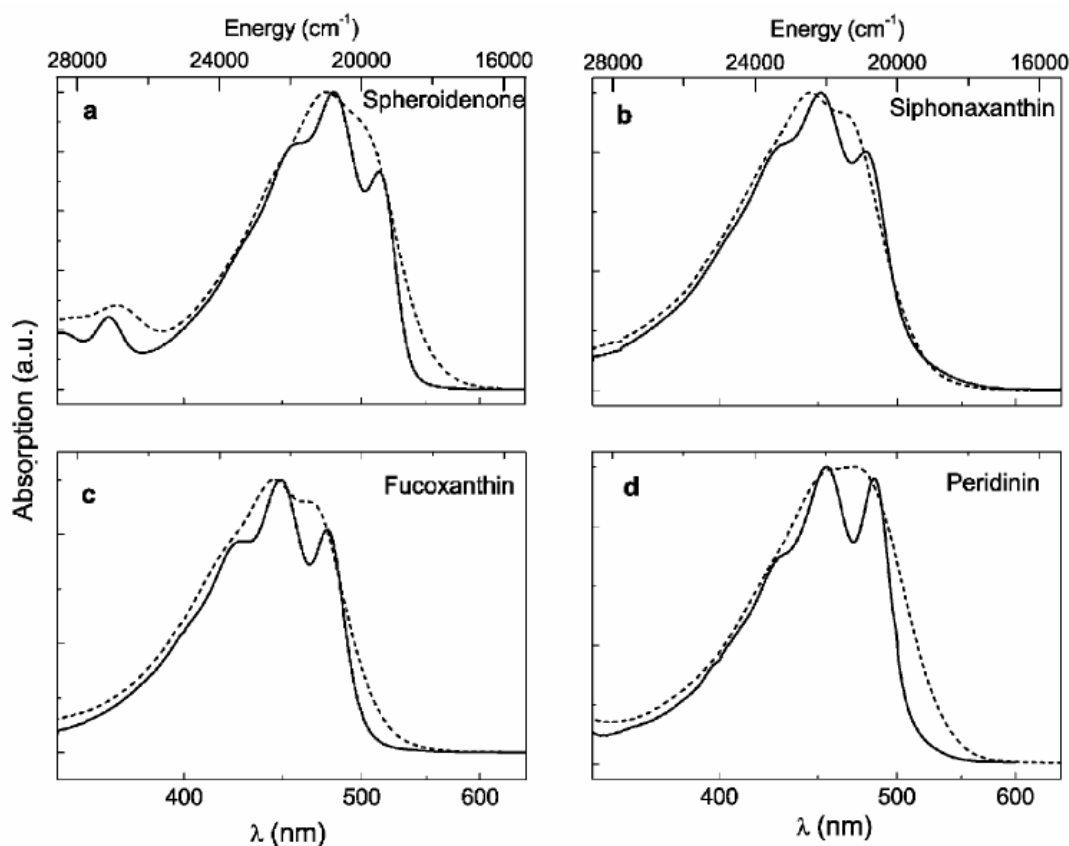
Fig.: 2 Room temperature absorption spectra of selected carbonyl carotenoids in non-polar (solid line) and polar (dashed line) solvents [18]. The broad band with more or less recognizable vibration sub-bands is characteristic of the $S_0 - S_2$ transition.

After promotion to the S_2 state, a carotenoid molecule undergoes fast relaxation (50 – 300 fs [2]) to the S_1 state. Consequently, this state is crucial for the energy transfer processes. Energy of this state also decreases with increasing of the conjugation length, but this dependence is slightly steeper than for the S_2 state, making the $S_2 - S_1$ gap larger for the longer carotenoids. Energy of the S_1 state vary from 11 560 cm^{-1} (856 nm) for spirilloxanthin to 16 520 cm^{-1} (605 nm) for fucoxanthin. Because it is a dark state inaccessible by the standard absorption or fluorescence spectroscopy, the other sophisticated methods are necessary to determine energy and lifetime of the S_1 state [2]. For the non-carbonyl carotenoids, the S_1 lifetime ranges from 1.4 ps for spirilloxanthin to 35 ps for neoxanthin. Properties of the S_1 state of carbonyl carotenoids are even more dependent on the solvent than in the case of the S_2 state. A significant shortening of the S_1 lifetime in polar environment is typical of carbonyl carotenoids with conjugation length N<10 (1.2). Because the most thoroughly studied carbonyl carotenoid is the peridinin that is the key pigment in PCP, its excited state properties will be described in a separate chapter (1.2).

1.2 Peridinin

Peridinin is a highly substituted carbonyl carotenoid. It is the most thoroughly studied carbonyl containing carotenoid because of its abundance in the light harvesting systems of marine algae and its strong solvent dependence of spectroscopic properties. Its S_2 energy is 20 620 cm^{-1} (484 nm) in n-hexane. The absorption spectrum is asymmetrically broadened to the red in polar environment. Using near-infrared time-resolved or fluorescence spectroscopy, the S_1 energy was located at 16 700 cm^{-1} (599 nm) in n-hexane and 16 200 cm^{-1} (617 nm) in methanol. Lifetime of the S_1 state was determined to be 160 ps in a non-polar solvent (e.g. n-hexane or CS_2), but decreasing significantly to 77 ps in the moderate polarity solvent tetrahydrofuran, to 54 ps in 2-propanol, and to even 10 ps in the polar solvent methanol. This drastic change in lifetime was explained by postulating the existence of another excited state with a charge transfer character, the intramolecular charge transfer (ICT) state lying in the vicinity of the S_1 state. Polar environment stabilizes the ICT state and pushes it below the S_1 state, eventually causing a quenching of the S_1 state that leads to the observed decrease of its lifetime in polar solvents. Current most widely used hypothesis is that the S_1 and ICT states merge together to form a single state (called the S_1/ICT state), which has a complicated solvent dependent potential surface (Fig. 3). Nevertheless, the exact nature of this problem is still a subject of a debate. This is the reason why the S_1/ICT notation instead of simple S_1 is usually used in the context of peridinin action in light harvesting antennas. This notation will be used also in this thesis.
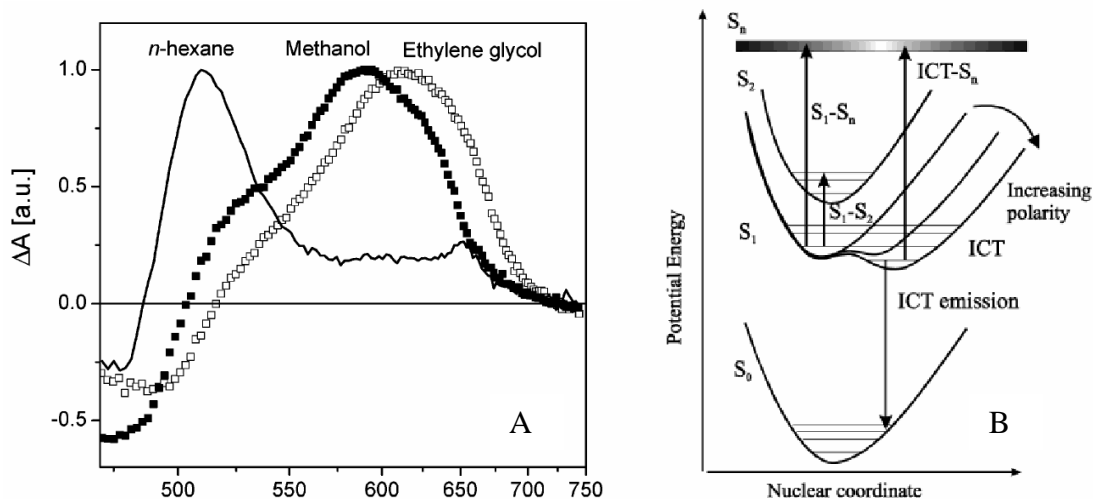
Fig.: 3 Transient absorption spectra of peridinin in solvents of different polarity (A) and a model of peridinin excited states in terms of potential surfaces (B). Diagram shows the polarity effect on the structure of the S_1/ICT potential surface of the peridinin molecule. The transitions which can take place in the molecule are denoted by arrows. Because of the lack of knowledge about the S_n potential surface, it is visualized only as a line representing a final state for S_1 - S_n and ICT-S_n transitions [25].
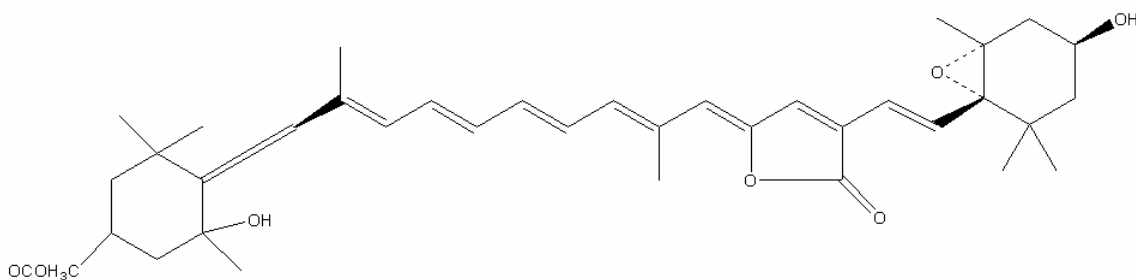
Fig.: 4 Molecular structure of peridinin

1.3 Peridinin chlorophyll protein (PCP)

A specific case of an antenna in which carotenoids are major light harvesting pigments can be found in a marine dinoflagellate *Amphidinium carterae* [4]. Its outer, water-soluble light harvesting protein is commonly termed the peridinin-chlorophyll-a protein (PCP), and its main pigment is a highly-substituted carbonyl carotenoid peridinin, whose light-harvesting capacity is further extended by the presence of chlorophyll-a molecules. This protein is sometimes called the main form peridinin chlorophyll protein (MFPCP), because other forms of PCP were isolated. It is especially the so called high-salt peridinin chlorophyll protein (HSPCP). This protein is similar to the MFPCP, but

contains only six peridinins. This thesis deals only with the MFPCP so only the shorter PCP abbreviation is used.
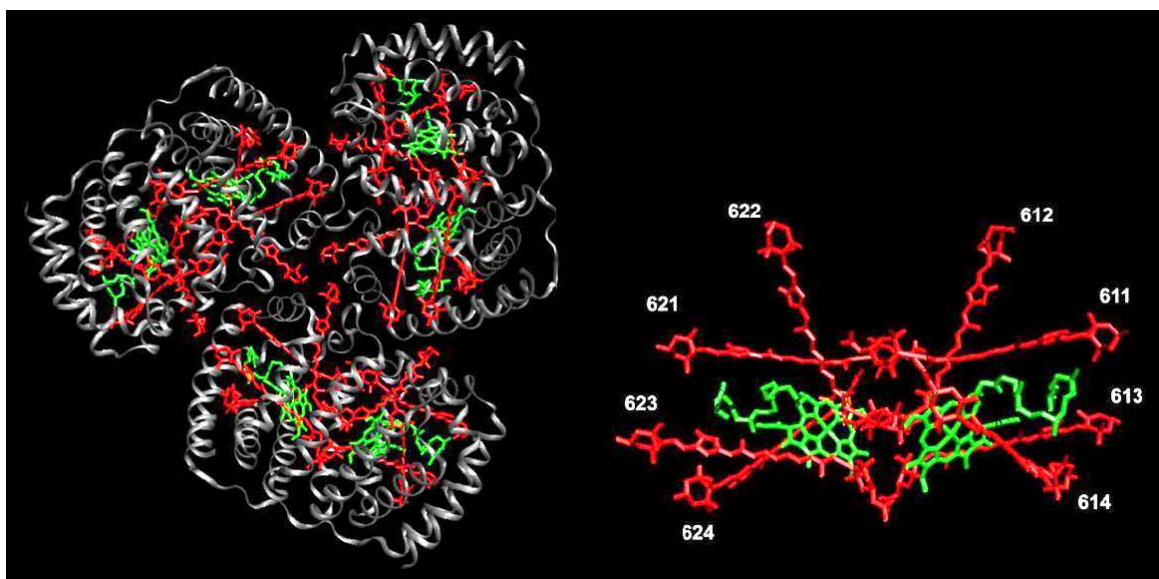
Fig.: 5 Left: Trimer of PCP proteins. Right: Orientation of pigments inside of single PCP complex and usual notation of peridinins inside.

PCP structure is known with 2Å resolution [5] so we have rather precise information about positions and distances of the pigments. PCP usually forms trimers of complexes consisting of two almost identical subunits, each containing 4 peridinins and one Chl-a molecule (Fig. 5). Distances between peridinins inside the subunit range from 4 to 11 Å. The closest distances between peridinins and tetrapyrrole rings of Chl-a are about 3.3 – 3.8 Å. The distance between Mg atoms of Chl-a of each subunit is 17.4 Å [3]. Such a close contact of pigments enables effective network of energy transfer between the pigments in PCP. A lot of effort has been devoted to disentangle this network during the past few years (Fig.: 6).
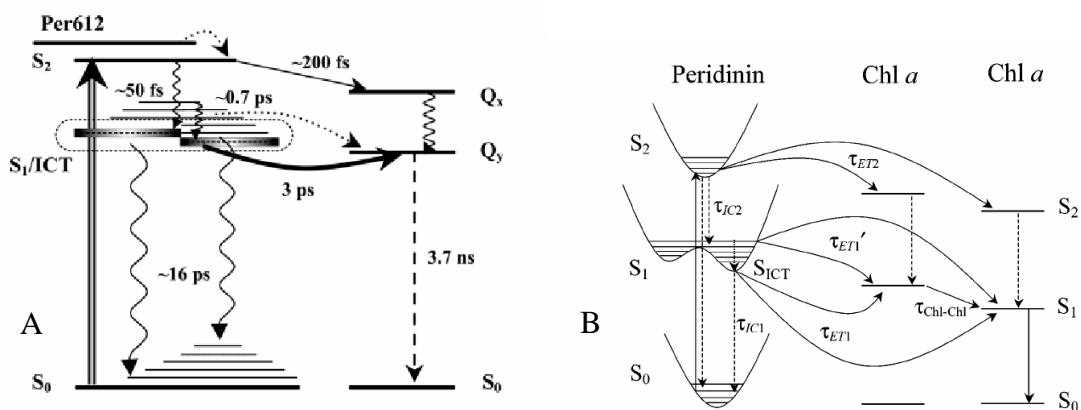
Fig.: 6 Simplified (A [2]) and detailed (B [27]) scheme of energy transfer pathways in the native PCP. Arrows denotes energy transfer pathways. Dashed or wavy arrows denote relaxation processes. Initial excitation is denoted by double arrow (A) or ordinary arrow (B).

It was discovered that the peridinins in PCP differ in their spectroscopic properties, but the question if they differ also in their function is still opened. Usually there were distinguished peridinins having their 0-0 bands of the S_0-S_2 transitions at 550, 535, 520 and 485 nm, but the actual values vary depending on the sources and methods used to obtain these values [7], [8], [9], [10]. Regardless the method, however, the blue shifted peridinins (0-0 peaks at 485 and 465 nm) can be distinguished, and these 'blue peridinins' were assigned to be peridinins 622 and 612 [2], [6], [16], (Fig.: 5).

Fig.: 7 Absorption spectrum of PCP. Note that the Soret peak of Chl-a peaking at 430 nm overlaps with the peridinin S_2 band.

Steady state spectrum of PCP consists of the typical broad carotenoid absorption band between 380 and 530 nm overlapped by Chl-a Soret absorption band at 438 nm (Fig.: 7). Chl-a Q_y band appears at 670 nm and very weak Q_x band at 615 nm.

1.4 Reconstituted PCP and goals of the thesis

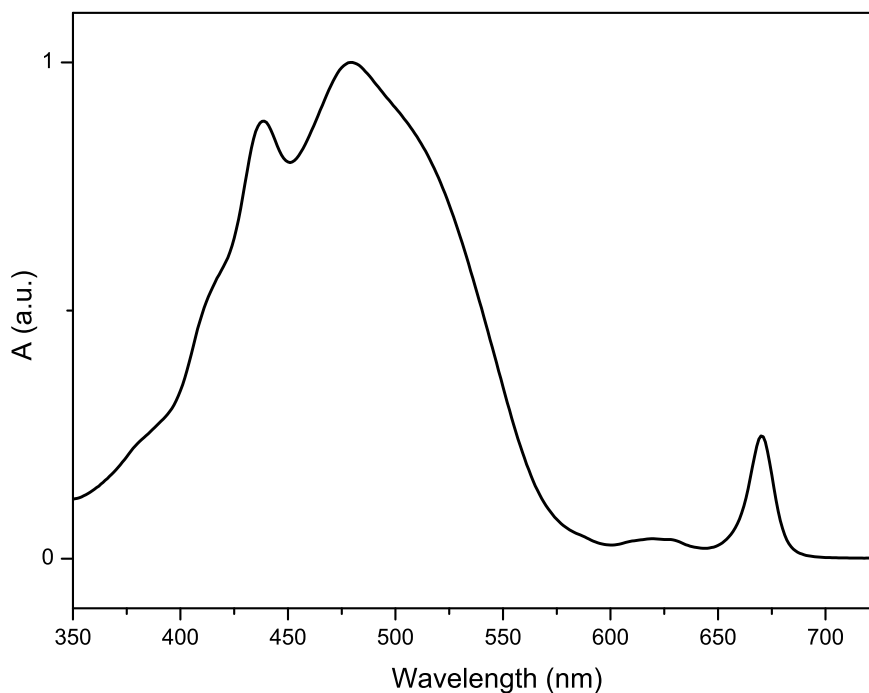Experiments confirmed that excitation energy absorbed by peridinins is transferred to chlorophylls, but a careful study of energy transfer pathways is complicated in native PCP, because of overlap of the Soret absorption band of chlorophyll-a (peaking around 438 nm) with peridinins (Fig.: 7) that significantly absorbs in the 400-550 nm region (Fig.: 2). This makes it difficult to excite selectively only desired molecules and the interpretation of resulting spectra becomes ambiguous as the excitation is moved to higher energies where the blue peridinins are expected to absorb. Recently, reconstituted PCP complexes with artificially substituted chlorophylls were prepared [11]. It was achieved by mixing of purified (by centrifugation or anion exchange chromatography) apoprotein expressed in *E. coli* with selected pigments at 4°C [11]. To reveal the potential role of the blue peridinins, the PCP complex reconstituted with Bchl-a is especially useful, because the Soret band of BChl-a peaks below 390 nm and it does not overlap with the peridinin absorption (Fig.: 2). Reconstituted PCP complexes substituted with Chl-b, Chl-d, acetyl-Chl-a, and Bchl-a were already studied [12]. Besides the PCP complexes reconstituted with a single chlorophyll species, hybrid PCP complexes containing different chlorophylls in each subunit were also prepared [13]. These complexes are useful for studies of the Chl – Chl energy transfer. In native complexes the two Chl-a molecules accommodated in the two subunits are nearly isoenergetic, making studies of energy transfer between them rather difficult. Thus, employing reconstituted PCP complexes in time-resolved studies enabled to fill some gaps in energy transfer schemes [2] (Fig.: 6), but there are still some unanswered questions, especially those dealing with detailed roles of individual peridinins (1.1).

This work aims at the study of the PCP substituted uniformly with Bchl-a and the PCP reconstituted with a Chl-b/Bchl-a mixture, resulting in a substantial fraction of PCP complexes having different chlorophyll in each subunit (Fig.: 8). The PCP complexes substituted by a mixture of Bchl-a and Chl-b have not yet been studied. The

combination of Bchl-a and Chl-b makes them suitable to test energy transfer mechanism between chlorophylls in PCP, because the energy gap between the Q_y bands is the largest achieved so far. The largest theoretical gap would be achieved by combining Chl-c and Bchl-b, but reconstitution of PCP with this combination has not yet been successful. To summarize, the main goals of this thesis focuses on application of the femtosecond time-resolved pump-probe spectroscopy (2.) to find a solution of the following two problems:

  First, to track paths of energy transfer inside the PCP reconstituted with Bchl-a in one domain and Chl-b in the second domain, and by the use of fitting methods find the time constants of the energy transfer. The key task is to find the possible energy transfer between chlorophyll molecules (3.1.1), and try to compare results with those predicted by calculations according to the Förster theory [14] (3.1.2).

  Second, to study dependence of excited-state dynamics of the PCP reconstituted with Bchl-a on excitation wavelength, and to find if it is possible to resolve differences in energy transfer pathways when some of the peridinins are excited selectively (3.2). For proper treatment of this problem a global fitting method was used (2.3).
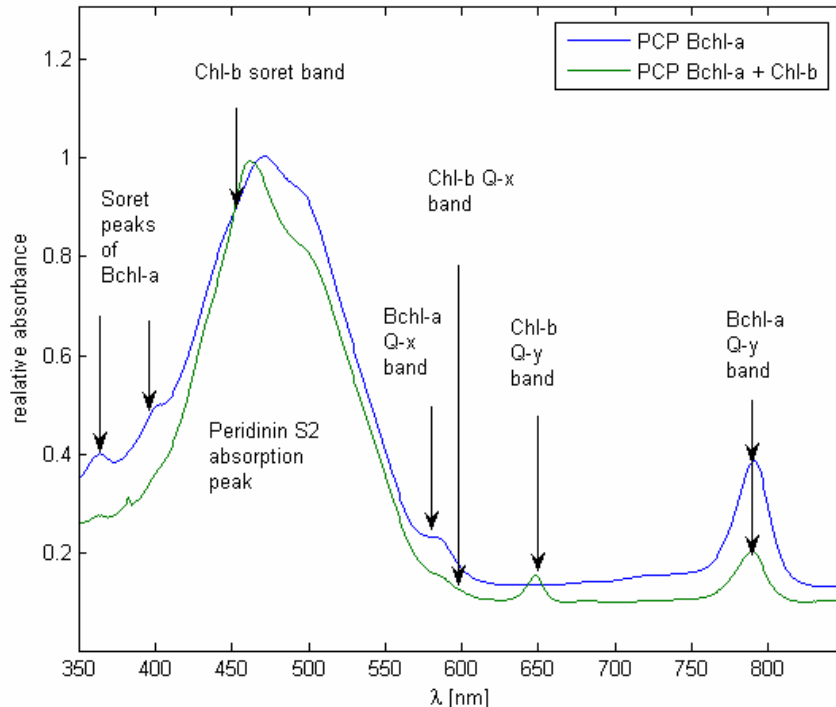

Fig.: 8 Absorption spectra of PCP reconstituted with Bchl-a (blue), and with mixture of Bchl-a and Chl-b (green) used for the experiments described in this thesis.

2. Methods

Femtosecond time resolved spectroscopy is a powerful method for studying the dynamics of excited states of molecules. There are several specific methods of the time resolved spectroscopy, each aiming at obtaining slightly different information about excited-state dynamics of the studied sample. In this thesis, a method called "pump-probe" or transient absorption spectroscopy was exclusively used. Principal description of this method is described in the following paragraphs with a brief reference to other related methods.

The main principle of the pump-probe spectroscopy is following: the sample is excited with a short, usually of sub-100 fs duration, laser pulse (the "pump" pulse), and then the absorption changes in the sample are measured after a well-defined time delay by another, usually polychromatic, pulse (the "probe" pulse) (Fig.: 9). As the time delay between the pump and probe pulses changes, the absorption of the sample changes, too. By systematic scanning the time delay between the pulses from zero (or better from a negative time when the probe pulse precedes the pump pulse and no signal is expected) to a desirable delay (usually up to 1 ns) we can record how the absorption changes induced by the pump pulse evolve in time. The time resolution is given by the time duration of the pump and probe pulses, though sophisticated deconvolution methods allow extracting time components even slightly shorter than the pulse duration. The time evolution of the absorption changes induced by excitation consequently can give us a clue to understanding of the involved photo-physical and photochemical processes. Technically, setting of the time delay between the pulses with a femtosecond precision is achieved by splitting one pulse in two (pump and probe), and letting the probe beam approach the sample by a longer path then the pump pulse. In such a case, the time delay between pump and probe will be $n(l_1 - l_2) / c$ where n is refractive index of the medium in which the beams propagate, $l_{1,2}$ are the lengths of the probe and pump paths, respectively, and c is the speed of light in vacuum. To set the delay, we conveniently use the instrument called "delay line" which is a corner reflector placed on a stepper motor controlled moving stage. The complication with this approach arises when using the polychromatic probe pulses, because refractive index n differs for each wavelength. Consequently, the actual time delay is different for each wavelength. This effect is

generally called a chirp. The chirp is strong especially when the beam travels through the lenses, filters or other optical components with high refractive index. We usually try to minimize the chirp by using reflective components like parabolic and/or spherical mirrors or partially reflecting mirrors instead of lenses, filters and other transmission components. A residual chirp can be suppressed by an appropriate data processing, but it is always better to minimize this effect in the measurement as much as possible.

lens
grating
mirror
beam splitter
1   laser source
2   light converter
3   sapphire plate
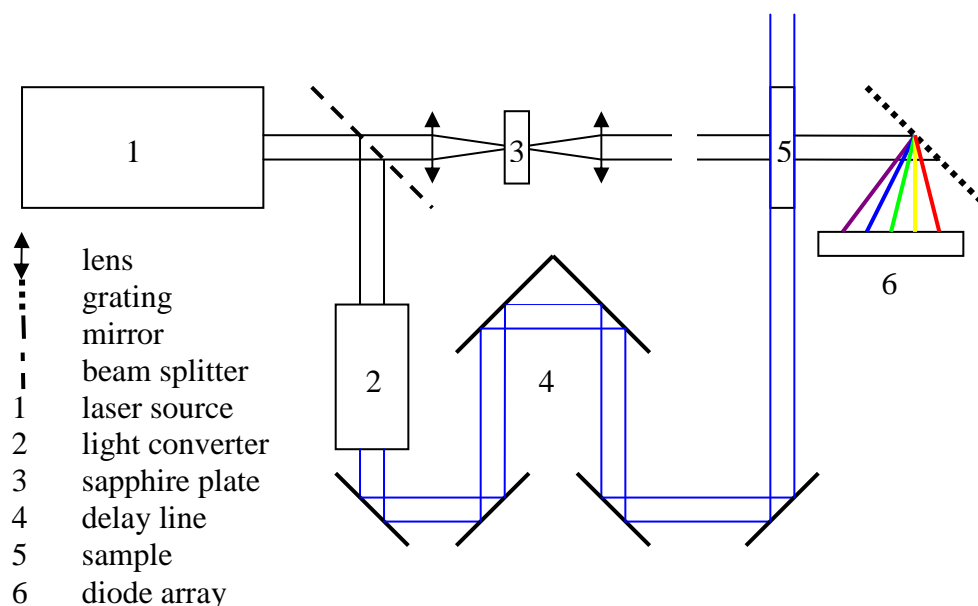4   delay line
5   sample
6   diode array

Fig.: 9 A block scheme of the basic principle of the pump probe experimental set-up. Primary beam generated by a femtosecond laser is split into two by a beamsplitter. The pump beam is converted to desirable excitation frequency. The probe beam is, with a help of certain nonlinear processes occurring in various materials (water, sapphire or other medium…) converted to a white light continuum. The time delay between the pump and probe is adjusted by spatial prolonging the path of one of the pulses, usually the probe beam.

There are number of other time-resolved methods like for example the pump-dump-probe spectroscopy, stimulated Raman spectroscopy and many others that, by using of more than one pump pulse, allow to study states that are not accessible by a single photon excitation, or to obtain different information about the excited-state properties of the sample. Although additional pump pulse brings a number of technical complications, the underlying principle of these methods is the same as in the pump-probe spectroscopy. Recently, also methods based on a coherent interaction of multiple pulses were developed. Among those, photon echo spectroscopy and two-dimensional optical spectroscopy are the most promising ones. These methods use the principles (described by the optical Bloch equations [28]) following from a fully-solved two-level

(or even more extended) quantum system, which are common in NMR spectroscopy. The amount of information obtainable by these methods is enormous, but these experiments, and especially their interpretations, have many pitfalls, which are negligible in NMR. These problems are related mostly to the very fast free induction decay of electronic states and short pulse wavelengths in comparison with the sample size (causing inhomogeneous excitation of the sample). These methods are currently at the front of research in time-resolved spectroscopy and near future will show if their potential can be fully exploited also in studies of excited-state properties of complicated systems such as light-harvesting proteins.

The crucial component of the time resolved spectrometer is a laser producing very short light pulses. This made femtosecond spectroscopy highly dependent on the development of the laser physics and made it impossible until about 25 years ago. The time resolution is approximately equal to the duration of the pulse. Enormous development of lasers generating ultrashort pulses in the past decade has witnessed construction of lasers delivering pulses going even to the attosecond regime, but pulses of such a short duration exceed limits of usability in a spectroscopy of biological systems. There are two main reasons for it. One is technical and the second is fundamental. The former one is that it is difficult to scan a time profile of such a short pluses and to measure their duration with required precision, which is very bad for the interpretation of measurements. The latter is that according to the uncertainty principle ($\Delta E \Delta t \sim h$) a visible light pulse of one femtosecond duration produces uncertainty in the spectral resolution of at least 300 nm. This makes a selective excitation hard or even impossible for biological molecules. Yet, there are ways how to, at least partially, circumvent this uncertainty. For example the femtosecond stimulated Raman spectroscopy uses a combination of a picosecond, spectrally narrow Raman pulse and a stimulating femtosecond spectrally broad probe pulse. This combination sophistically keeps the femtosecond time resolution, while allowing the spectral resolution to be determined by the Raman pulse. This approach can circumvent the uncertainty principle by an order of magnitude [26]. In fact, the uncertainty principle is of course not broken in this case, but rather bypassed in a tricky way. Although extremely interesting, none of these sophisticated time-resolved methods was employed for studies in this thesis. All experiments treated in this thesis employed standard pump-probe spectroscopy using a laser system generating pulses of ~150 fs duration, which makes problems with

the uncertainty principle acceptable (approximately 2 nm of spectral uncertainty in the spectral region of our measurements).

2.1 Description of the experimental set up

As mentioned in the preceding chapter, the measurement is technically performed by dividing the pulse into two beams called pump and probe. Because the primary laser generating ultrashort pulses is usually not tunable or tunable only to a certain extent, the pump beam is converted to the wavelength desired for excitation by the use of a nonlinear parametric amplifier. This instrument generates (by the use of nonlinear optical effects in an appropriate crystal) parametric frequencies from the primary beam. The actual frequencies of the parametric beams (signal and idler) depend on the angle of the nonlinear crystal. By amplifying, mixing and generating higher harmonic frequencies of the parametric light it is possible to produce almost arbitrary frequency from the near-UV to the mid-IR range. Some of the original laser frequency goes through, and an appropriate filter should be placed into the beam to block the original frequency while the desired frequency generated in the parametric amplifier will pass. After preparing the appropriate pump frequency, the pump beam is led through the delay line. This allows an adjustment of the time delay without changing any other parts of the experimental setup. The precise movement of the delay line is achieved by a computer controlled step motor, because we need the precision in spatial position in the μm range to maintain the time resolution in the sub-100 fs range. Then the pump is led through the Berek polarization rotator, which by the use of a λ/2 plate rotates the polarization plane of the pump beam by an appropriate angle to set the mutual polarizations of the pump and probe beams to a desired angle.
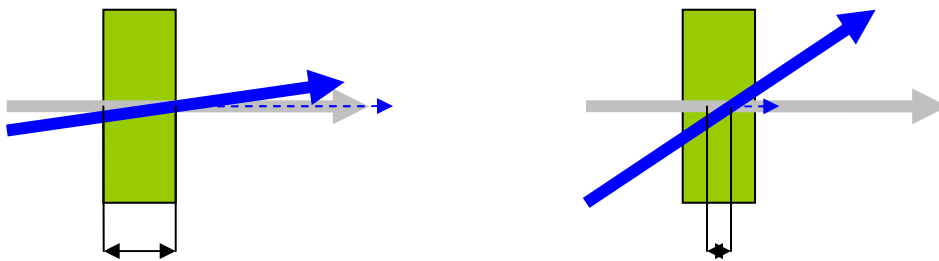

Fig.: 10 Dependence of the pump-probe overlapping depth on the angle between the pump and probe beams. The pump beam is represented by a blue arrow, probe by a grey arrow. Width of the overlapping region is denoted by double arrows. Small angle allows longer overlap and

consequently stronger signal. Large angle causes shorter overlap but smaller dispersion toward the probe direction.

Finally, the pump beam is focused on the sample to a spot of ~500 μm diameter that overlaps with the probe beam. The larger the angle between the pump and probe beams at the sample, the less pump light is diffracted to the detector. On the other hand, the smaller the angle the stronger signal is obtained, because, due to a certain thickness of the sample, the overlapping space will be longer (Fig. 10). The actual angle is set to find a compromise in a particular experiment and parameters of the sample (scattering media requires larger angle; samples with low optical density gave better results with smaller angle).
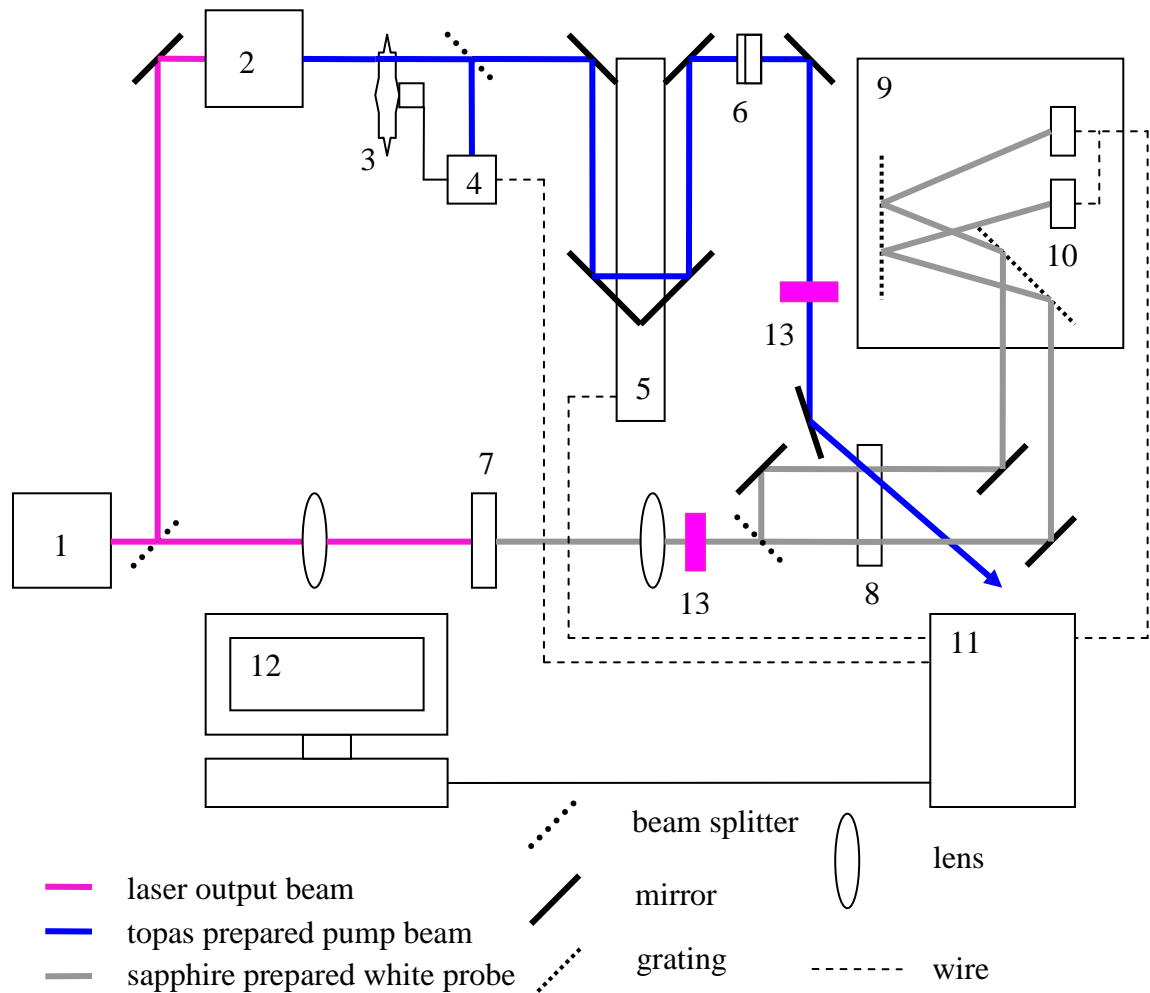

Fig.: 11 Scheme of the used pump-probe experiment. 1-main laser (Integra-I) 2-parametric amplifier (Topas) 3-chopper 4-chopper synchronizing PIN diode 5-delay line 6-Berek polarization rotator 7-sapphire plate 8-sample 9-spectrograph 10-diode arrays 11-main control box 12-computer 13- filter absorbing residuals of main laser frequency output.

The probe beam is converted to a white light continuum. It is usually done by focusing a fraction of the primary laser beam into an appropriate medium (sapphire, quartz, CaF_2, water…), in which nonlinear effects start to dominate to create a smooth spectral distribution. The residual original frequency is suppressed by a cut-off filter. The choice of the medium depends on the probing spectral region. In order to improve the signal-to-noise ratio further, the probe beam is divided into two, one of which does not overlap with the pump beam and serves as a reference for the final absorption measurement. Both reference and probe beams are focused on the sample, and led through the sample at the entrance slit of a spectrograph. Focusing into the sample is achieved by spherical mirrors instead of lenses to minimize the chirp of the probe beam. In the spectrograph employing a single grating, both beams are dispersed onto two diode arrays, each comprising of 1024 photodiodes, allowing recording the whole spectrum simultaneously. Diode arrays are connected with the data acquisition software that further processes the signal and calculate the transient absorption spectra.

To reach the maximal signal to noise ratio, effects of the time fluctuation of both the pump and probe beam should be minimized. This is fixed by the use of synchronised detection. A chopper is placed in the path of the pump beam, and chopper frequency is synchronized with the laser repetition rate to block every second pulse. Using this arrangement, measurement of the sample absorption with and without the pump is continuously repeated with a very high frequency. This sets an individual reference to each spectral probe measurement and minimises the effects of fluctuation over the longer time durations. To improve the signal to noise ratio even further, usually a large number of cycles is repeated and averaged. If the noise has a Gaussian distribution the signal to noise ratio should increase with the square root of number of averaged measurements (this means that for example average of one hundred measurements should decrease the noise ten times). Eventually, the transient absorption spectra (TAS) are computed from measured parameters according to the following equation

$$TAS = log\ ((I_p/I_{0p})/(I_n/I_{0n})) = log(I_p/I_{0p}) - log(I_n/I_{0n}) = A_{pumped} - A_{non\text{-}pumped}$$

where I_p, I_n are the intensities of the probe beam with and without pump, respectively, and I_{0p}, I_{0n} are corresponding reference intensities. From the expression follows that TAS is in principle the absorbance with pump minus absorbance without pump. The

TAS is recorded for different time delays to form a matrix with one dimension indexing the wavelength and the second indexing the time delay (Fig.: 12).

Because it is desirable to excite all probed molecules the pump beam should be more intense than the probe beam. This brings a problem with potential sample degradation during the measurement. It is usually solved by the mixing the sample inside a cuvette, or by shaking or rotating the whole cuvette. Rotating cuvettes spinning at a rate ensuring that each excitation pulse hits a fresh sample are commonly used in transient absorption measurements. For these purposes, circular rather than rectangular cuvettes are usually used. On the other hand, since the rotating cuvette could be a considerable source of noise, it is always important to test the sample stability and decide how intensive mixing is necessary.
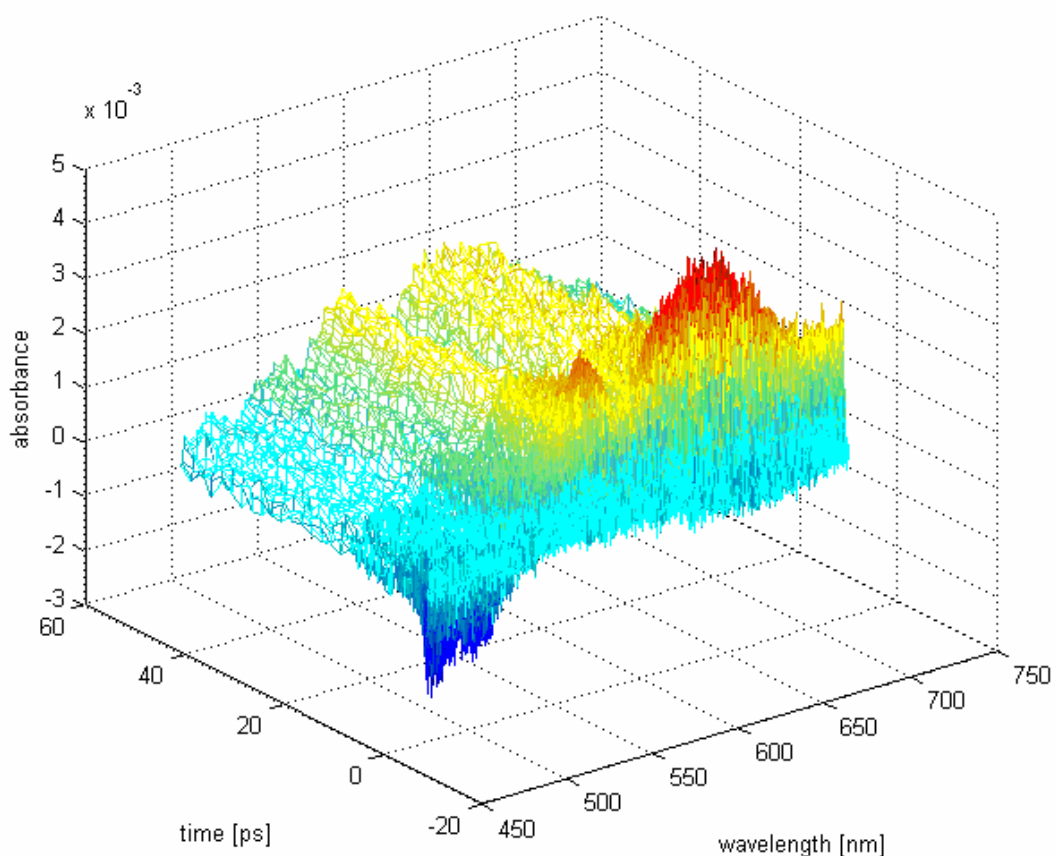

Fig.: 12 Transient absorption data of PCP reconstituted with Bchl-a excited at 390 nm.

2.2 Technical parameters of the individual experiments

Measurements presented in this thesis were performed on a femtosecond laser system consisting of a primary laser Integra-I (Quantronix). The output pulses, delivered at a repetition rate of 1 kHz, have ~130 fs duration, an average energy of ~2 mJ/pulse and a central wavelength of 780 nm. The pump beam was prepared in the optical parametric amplifier (Topas, Light Conversion), allowing tunability of the pump wavelengths approximately from 250 nm to 2000 nm. The white-light probe beam was generated by focusing a fraction of the primary laser output into a 3 mm sapphire plate by a lens of 10 cm focal length. The sapphire creates spectral continuum in the range of 450 – 780 nm. Both the pump and probe beams were linearly polarized with the mutual angle set to magic angle (54.7°) by the Berek polarization rotator to avoid anisotropic effects. The part of the setup as described above was used for all experiments. Other details differ slightly among individual experiments. All experiments presented in this thesis can be divided into two parts. The first one deals with measurements of PCP reconstituted with a single chlorophyll species, Bchl-a (2.2.1), the second describes experiments with PCP reconstituted with mixed chlorophyll sites, containing Bchl-a and Chl-b (2.2.2). Because a different experimental setup was used for these two sets of experiments, the details regarding individual experiments are described in next Chapters.

2.2.1 Experiment on PCP reconstituted with bacteriochlorophyll-a

The sample was inserted into a rotating cuvette consisting of two 1 mm quartz plates separated by a 1 mm Teflon spacer. The PCP complexes, that were stored in dark at -80 °C prior to experiments, were dissolved in a buffer (25 mM Tris pH 7.5, 2 mM KCl) to achieve optical density of about 0.2 at 470 nm. The pump beam was set to wavelengths 390, 430, 470, and 530 nm (Fig.: 13) to excite different peridinins in the PCP complex.
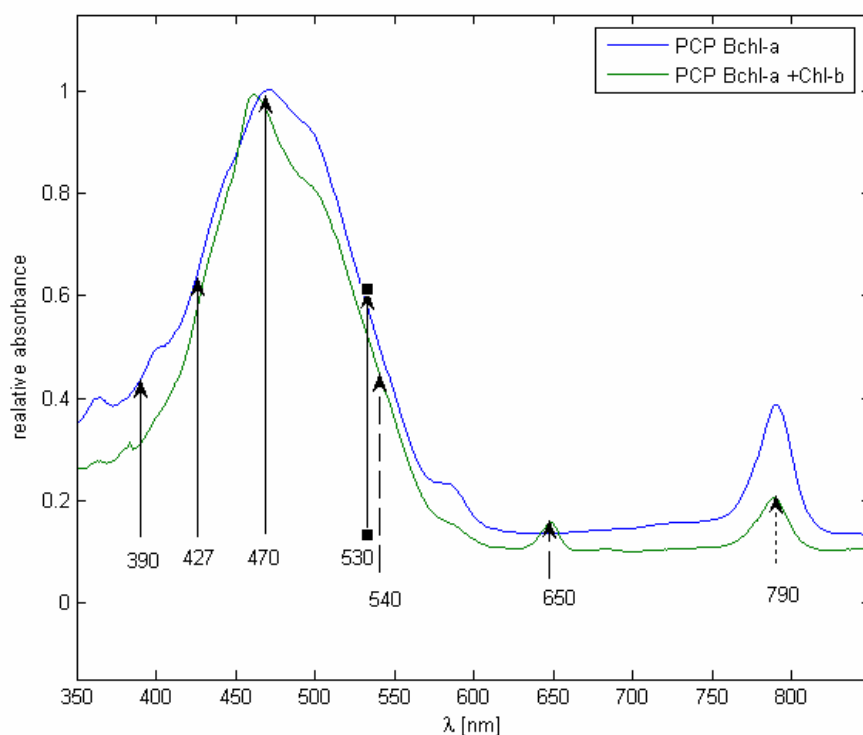
Fig.: 13 Choice of excitation wavelengths in the Bchl-a experiment (full arrows) and in the Bchl-a + Chl-b experiment (dashed arrows). The probing wavelength used in the Bchl-a + Chl-b experiment is shown as dotted arrow.

The resulting transient absorption was recorded by a 1024-element diode array set to monitor the spectral region between 476 and 718 nm. All measurements were carried out at room temperature with the same sample that was kept in dark at 4 ˚C between individual measurements. Absorption spectra were recorded before and after each measurement to examine the sample degradation.

2.2.2 Experiment on PCP reconstituted with chlorophyll-b and bacteriochlorophyll-a

The sample was placed into a standard 2 mm quartz cuvette. The concentration was adjusted to spectral density of 0.5 at 470 nm using the same buffer as used for the PCP complex reconstituted with Bchl-a. The pump beam was set to excite either red-absorbing peridinin at 540 nm to follow the peridinin-Chl energy transfer or to excite Chl-b at 650 nm to monitor the energy transfer between the two chlorophyll species. In this case, probing was achieved by a single-diode detector with a probe wavelength

fixed to the standard main laser output (786 nm), because it matches well the Bchl-a Q_y band (Fig.: 13). Effects of mixed site reconstitution are discussed in the Results section.

2.3 Global fitting analysis

Global fitting analysis is a method of analysing the time resolved spectra [20]. It uses the fact that spectra of an arbitrary origin consist of bands which usually overlap each other, but evolve in time in a different way. It is also possible to resolve several exponentials in the evolution of intensity at selected wavelength (3.1.3), but with the increasing noise and complexity of the overlapping components this approach becomes insufficient. In that case the global fitting resolves the problem by creating the model consisting of definite number of spectral components with certain spectra that evolve one in another in a defined way, and fitting this model into the data. It is also possible (and very usable) to fix some parameters of the model according to knowledge or a theory (both constants of time evolution and spectra of a selected component can be set); and let other components be fitted. This enables to test the theories or simply to increase the accuracy of the fit.

The data collected in the experiments described here were fitted globally by the commercially available fitting software (DAFit (Pascher Instruments)). This program enables only a limited number of functions. Generally, the program allows creating a model based on an arbitrary number of successive components evolving one to another and fit it to the data. It means that for all j wavelengths the data are fitted with a sum of i exponentials:

$$\sum_j \sum_i a_{ij} \cdot e^{-k_i t}$$

where a_j represents the spectrum of each time component. For the last component, k set to zero so this component does not evolve in time and represents merely a final state of the transition process. This program enables to fix an arbitrary constant k_i, but it does not allow setting the spectrum of the component or fitting the model in which branching processes take place. Yet, this program allowed to fit multiexponential decays to the recorded data for all studied excitation wavelengths for the PCP reconstituted with Bchl-a, and look for the correspondence of fitted components with the known spectra of peridinin states (1.2) and Bchl-a. This program also allows suppressing the chirp in the data caused by the spectral dispersion in an experimental apparatus (2.).

3. Results and discussion

The section Results is divided into two separate parts. The first deals with the PCP heterogeneously reconstituted with Bchl-a and Chl-b (3.1), and the second describes experiments with the PCP homogeneously reconstituted with Bchl-a (3.2).

3.1 Energy transfer in PCP reconstituted with a mixture of chlorophyll-b and bacteriochlorophyll-a

Two possible energy transfer routes were studied; energy transfer from Chl-b to Bchl-a achieved by a selective excitation of Chl-b at 650 nm, and energy transfer from peridinins to Bchl-a initiated by excitation of peridinins at 540 nm. The former is more straightforward and will be treated first.

At the beginning of this section it is appropriate to discuss the possible effects of the mixed site reconstitution. Because the initial ratio of molar concentrations used for the reconstitution was Bchl-a : Chl-b equal 3 : 1, it is possible to make an approximate estimate of affinity to PCP of these pigments from the measured absorption spectra. If P(Chl-b) represents probability of reconstitution as the measure of Chl-b affinity, similarly P(Bchl-a) mirrors the binding affinity of Bchl-a, and the height of their Q_y peaks for the same molar concentration is known, the expression which should hold is the equation :

$$\frac{0.75 \cdot P(Bchl-a)}{0.25 \cdot P(Chl-b)} = \frac{Q_y(Bchl-a)}{Q_y(Chl-b)}.$$

The amplitudes of Q_y peaks obtained from the absorption spectra set the right side of the equation equal 1.8 which produces the ratio of affinities equal 0.4:

$$\frac{P(Bchl-a)}{P(Chl-b)} = 0.4$$

This result suggests the affinity of Bchl-a significantly smaller than that of Chl-b. Further analysis of this problem is blurred by the fact that absorption of the sample was measured without carefully prepared reference sample. The amplitudes of Q_y peaks need an accurately defined baseline to calculate the ratio exactly. The same cuvette as used for the measurement with PCP without any chlorophylls would be appropriate for

it but the sample of pure PCP apoprotein was not available for reference measurements. However, although this can slightly change the affinity ratio, in no way it can affect the conclusion about higher Chl-b affinity.

From the calculated affinity an approximate distribution of different PCP reconstitution can be calculated by the use of the basic probability principles:

1) Both sides reconstituted by Chl-b: $(0.25 \cdot P(Chl\text{-}b))^2$ ~21%

2) Mixed site reconstituted: $(0.25 \cdot 0.75 \cdot P(Chl\text{-}b) \cdot P(Bchl\text{-}a)) \cdot 2$ ~50%

3) Both sides reconstituted by Bchl-a: $(0.75 \cdot P(Bchl\text{-}a))^2$ ~29%

The results suggest approximately a half of the PCP in the sample reconstituted by mixed sites. If the transition from Chl-b to Bchl-a is measured, only these complexes brings signal while the other excited molecules containing pure Bchl-a contributes by constant absorption to the whole Bchl-a transient spectrum. The time constant of the exponential should not be in principle affected, but the noise could be higher because of the higher background.

In the experiment where peridinin Bchl-a transfer was recorded 79 % of molecules should respond for the pump. But it should be kept in mind that about two thirds of the signal originates from mixed sites reconstituted PCP while the remaining third of signal originates from PCP homogenously reconstituted by Bchl-a.

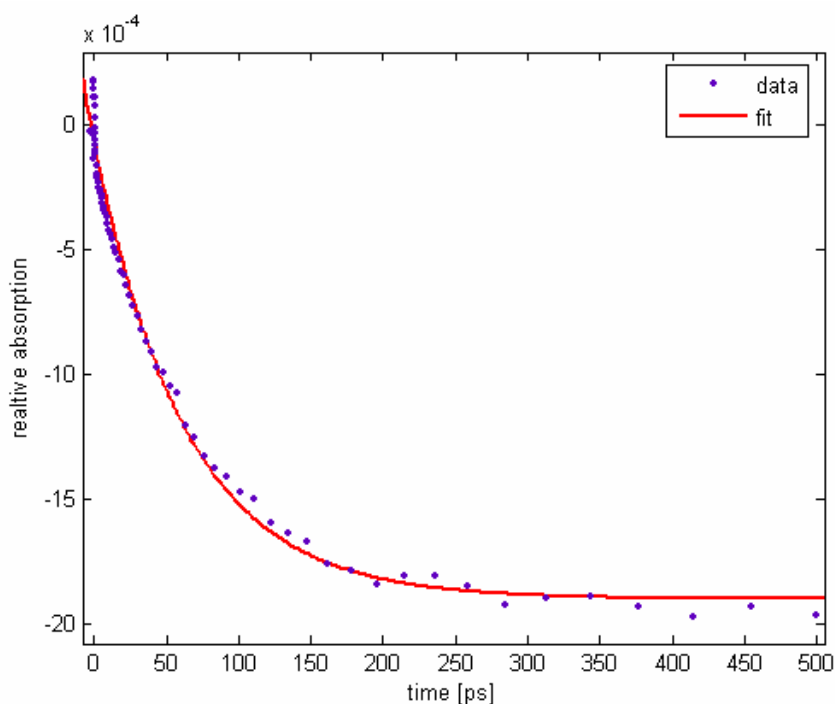### 3.1.1 Energy transfer from Chl-b to Bchl-a

Fig.: 14 Experimental data and a single-exponential of the Chl-b to Bchl-a energy transfer recorded on PCP reconstituted with Bchl-a and Chl-b excited at 650 nm and probed at 790 nm.

Energy transfer from Chl-b to Bchl-a was studied by the selective excitation of Chl-b Q_y absorption band at 650 nm, while bleaching of the Bchl-a Q_y band at 786 nm, signalling arrival of excitations to Bchl-a, was monitored (2.2.2). From PCP absorption spectra it is obvious that peridinin excitation can be in this case neglected, because peridinin absorption at 650 nm is virtually zero (Fig.: 1). The experimental results, shown in Fig. 14, can be fitted by a single-exponential curve of the form: $ae^{-kx} - c$.

Small disagreement of the fit with the data could be, however, seen especially in the first few ps. This is a characteristic of all kinetics recorded on PCP and it is related to the ultrafast relaxation processes occurring in the initially excited molecule. Part of the mismatch is likely caused by the direct excitation of Bchl-a, because the absorption bands extends to 650 nm (Fig. 15). The mentioned disagreement is, however, beyond the standard error of the measurement so its discussion is questionable. This fit sets the time constant of the energy transfer from Chl-b to Bchl-a to 64 ps with 95% trust region 59 – 70 ps. This is in a good agreement with a similar study published on PCP reconstituted with a mixture of Bchl-a and Chl-a, where a time constant of 59 ps was determined for Chl-a to Bchl-a energy transfer [13]. Although it may seem surprising

that comparable energy transfer times were found for Chl-b and Chl-a molecules serving as energy donors, the reason of such a small difference could be well explained by the Förster type energy transfer mechanism [14] (3.1.2).

3.1.2 Förster-type model of Chl-b – Bchl-a energy transfer

The Förster mechanism of an energy transfer operating via a dipole-dipole interaction predicts energy transfer rates between molecules [14]. The physical principle of this process is a coupling of oscillators and can be well explained in terms of the classical physics. Similar to the coupled classical oscillators, the efficiency of the energy transfer depends not only on the coupling strength, but also on the similarity of resonant frequencies of involved oscillators. Great advantage of the Förster theory is that it employs easily accessible quantities, emission spectrum of the donor and absorption spectrum of the acceptor to calculate the overlap integral that is a measure of the likeness of the resonant frequencies. In solution, the orientation and distance of the donor and acceptor is averaged. However, if the donor and acceptor are in a fixed position, like chlorophylls in PCP, the distance and orientation factors must be incorporated in the calculation. The Förster theory predicts a time constant of energy transfer between the donor and acceptor by the equation [14]:

$$\frac{1}{\tau} = 1.18 \left(C \frac{5.04 \mu_A \mu_D \kappa}{R^3} \right)^2 \Theta$$

where μ_A and μ_D are transition dipole moments that can be calculated from extinction coefficients as:

$$\mu = 0.12 \sqrt{\frac{\varepsilon_{max} \Gamma}{\nu_{max}}}$$

where ε_{max} is the extinction coefficient at maximum of the absorption band in $mol^{-1}.cm^{-1}$ units, Γ is a full width at the half maximum of the absorption band in cm^{-1}, and ν_{max} is energy of the absorption band maximum in cm^{-1}. C is a correction factor that takes into account the effects of medium and is set to 0.6 [13] for PCP; κ is an orientation factor and R is a distance between the centres of dipoles:

$$\kappa = 2\cos\theta_D \cos\theta_A + \sin\theta_D \sin\theta_A \cos\varphi$$
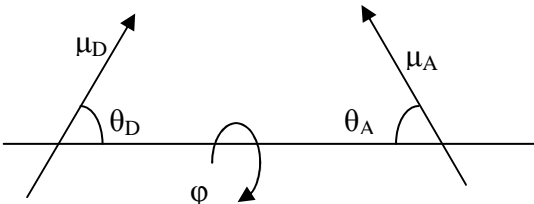
The value κ/R^3 is in practice difficult to determine, because the Q_y dipole is not exactly aligned along the diagonal of chlorophyll molecules [15]. Therefore, a value of $\kappa/R^3 = 0.103$ nm^{-3} taken from a thorough analysis of this problem [13] was used for calculation. Overlap integral is calculated by the equation:

$$\Theta = \int A(\nu) \cdot D(\nu) d\nu \qquad \text{for } A(\nu) = \frac{a(\nu)/\nu}{\int (a(\nu)/\nu) d\nu} \text{ and } D(\nu) = \frac{d(\nu)/\nu^3}{\int (d(\nu)/\nu^3) d\nu},$$

where $a(\nu)$ is the absorption spectrum of an acceptor and $d(\nu)$ the fluorescence spectrum of a donor. The calculated value obtained from the measured absorption and emission spectra using the above integrals is 1.13×10^{-4}.

These all parameters together yield the value of $\tau = 45$ ps. This is slightly less than the experimentally measured value of 64 ps, but it confirms the trend that Förster type calculations of τ performed on PCP usually predict shorter lifetimes than those obtained from experiment [13]. A brief look at the fluorescence and absorption spectra of Chl-b and Bchl-a, respectively, (Fig.: 15) clearly shows that the spectral overlap is achieved mostly via the vibronic bands of both involved molecules. This also explain why the Chl-b to Bchl-a energy transfer rate is so similar to the one obtained for Chl-a to Bchl-a energy transfer [13]. The different positions of the Q_y bands of Chl-a and Chl-b affect the overlap integral less than could be expected.
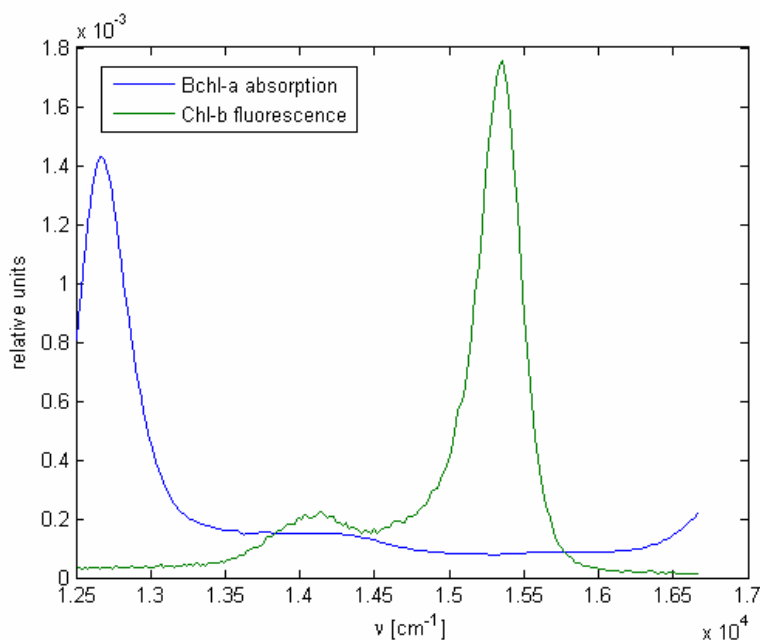
Fig.: 15 Bchl-a absorption and Chl-b emission spectra used for the Förster type energy transfer rates calculation. Note that the energy scale is in wave numbers as used for the calculation of spectral overlap. This makes the energy grow from left to right – opposite to most of the depicted graphs with energy scale in wavelengths.

3.1.3 Energy transfer from peridinins to Bchl-a

Energy transfer from peridinins to Bchl-a was studied in a way similar to the Chl-b to Bchl-a energy transfer. Peridinins were excited at 540 nm and Bchl-a Q_y bleaching signal was recorded. The situation is, however, more complicated in this case, because excitation is simultaneously transferred from peridinins to Chl-b, subsequently from Chl-b to Bchl-a, and also directly from peridinins to Bchl-a. Nevertheless, peridinin-Chl transfer is much faster [12] than Chl-Chl transfer (64 ps in this case). Thus, if the peridinin-Bchl-a transfer is considered to be much faster compared to the peridinin-Chl-b (9.4 ps [12]) and Chl-b-Bchl-a (64 ps), the data can be fitted by two independent exponentials with only a small error. When the faster process is almost finished, the slow one will be still almost at the beginning. This makes these processes, in the first approximation, separable. Fit of the data by a two-exponential function $a \cdot e^{-bt} + d \cdot e^{-et} + c$ is depicted in Fig. 16.
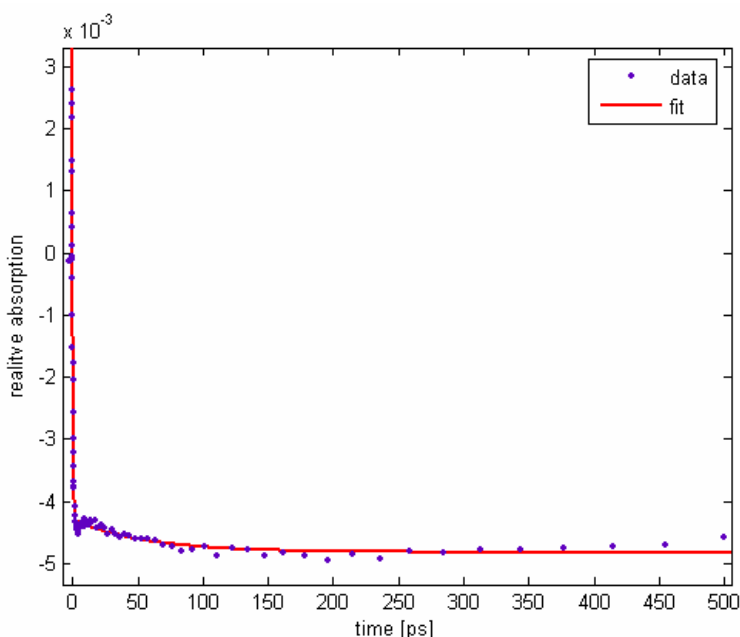
Fig.: 16 Experimental data and fit of the peridinin to Bchl-a energy transfer recorded for PCP reconstituted with Bchl-a and Chl-b excited at 540 nm and probed at 790 nm.

The curve can be easily divided into two parts where each of the involved processes is strictly dominant with only a small region where both energy transfers mix together. This model sets one lifetime to 0.37±0.4 ps (high uncertainty is a consequence of small time resolution compared to the process, this is one of the reasons why the more accurate global fitting is usually used (2.3)) and the second to 55±15 ps. This is in a satisfying agreement with the time constants of peridinin to Bchl-a energy transfer of 0.46 ps [12], [13], and the time constant of 64 ps determined in (3.1.1) for the Chl-b to Bchl-a energy transfer. The fact that both constants are below expected values is a logical consequence of ignoring the effects of the peridinin to Chl-b energy transfer, because this minor route contributes indirectly to the transition rate and makes it appear faster than actually is. We can perform a small correction on peridinin-Bchl-a transfer by the known peridinin-Chl-b time constant of 9.4 ps [12] with the use of $\tau^{-1} = \tau_1^{-1} + \tau_2^{-1}$ ($k = k_1 + k_2$). The principle is that the energy moves from peridinins not only directly to Bchl-a but also to Chl-b. A simple double-exponential fit does not take it in an account, but is possible to make the first order correction to the fitted values by subsequent accounting for the effect. The effect of neglecting branching in the energy transfer pathways is a source of uncertainty also in the global fitting if the branching is not involved directly in the model (3.2.2). If we account for the Chl-b to BChla energy transfer, the value of peridinin-Bchl-a time constant is changed to 0.39 ps. To perform

an exact correction, the solving of appropriate differential equations for the involved transitions is necessary. But even without solving and fitting appropriate differential equations it seems to me improbable that the carefully corrected value would rise to 0.46 ps measured on PCP reconstituted with Bchl-a only. On the other hand if we consider the standard error of the experimental data, the results are in a principal agreement with the results published earlier [12].

3.2 Energy transfer in of PCP homogenously reconstituted with bacteriochlorophyll-a

The first part of this section treats mostly the recorded transient absorption spectra alone and their qualitative analysis (3.2.1). The second part aims on the global fitting of the data (3.2.2) and interpretation of the fits. The third part is a brief comment to the sample degradation processes observed during measurements (3.2.3).

3.2.1 Transient absorption spectra

One of the aims of this work was to look for the dependences of transient absorption spectra (2.1, Fig. 12) and underlying excited-state dynamics on excitation wavelength. Because the peridinins in PCP are exposed to different environments, their spectroscopic properties should differ (1.2). Since this effect is manifested by different spectral origins of the 0-0 band of the S_0-S_2 transition (1.2), varying the excitation wavelength should affect transient absorption spectra in some way, as different peridinins will be predominantly excited at different excitation wavelengths. The problem is that the dependence of the S_2 state properties on polarity of the environment is rather small compared to the dramatic dependence of the S_1 state properties [2] (1.1). Consequently, even if the excited state dynamics of individual peridinins differ, a selective excitation is problematic as a consequence of the large overlap of the $S_0 - S_2$ transitions of peridinins in PCP (1.3, Fig. 7). According to the measurements performed on pure peridinin dissolved in solvents of different polarities [17], [18], (Fig. 2), it is expectable to find some differences while exciting in the region of 350-400 nm or 500-550 nm. Peridinins in the polar environment or those having a H-bonded conjugated

carbonyl group should absorb significantly at 550 nm, while peridinins experiencing less-polar environment should absorb only a little in this region. Even though the reconstitution with Bchl-a solves the problem of the overlap between the peridinin and Soret absorption bands, some complications may arise when exciting either at the very blue or the very red edge of peridinin absorption in PCP. The Soret band of Bchl-a peaks around 380 nm while the Q_x band has a distinct band at 585 nm. From this point of view the excitation wavelengths tuned to 390 and 530 nm seem to be a good compromise capable to excite selectively the blue and red shifted peridinins, respectively, while minimizing direct Bchl-a excitation. Another two wavelengths, 427 and 470 nm, were chosen to fill the gap between those values. At these wavelengths, only a small selectivity can be achieved, but they provide a useful reference for the 390 and 530 nm experiments. Slices through the most important times of recorded transient absorption spectra are shown in Fig. 17):
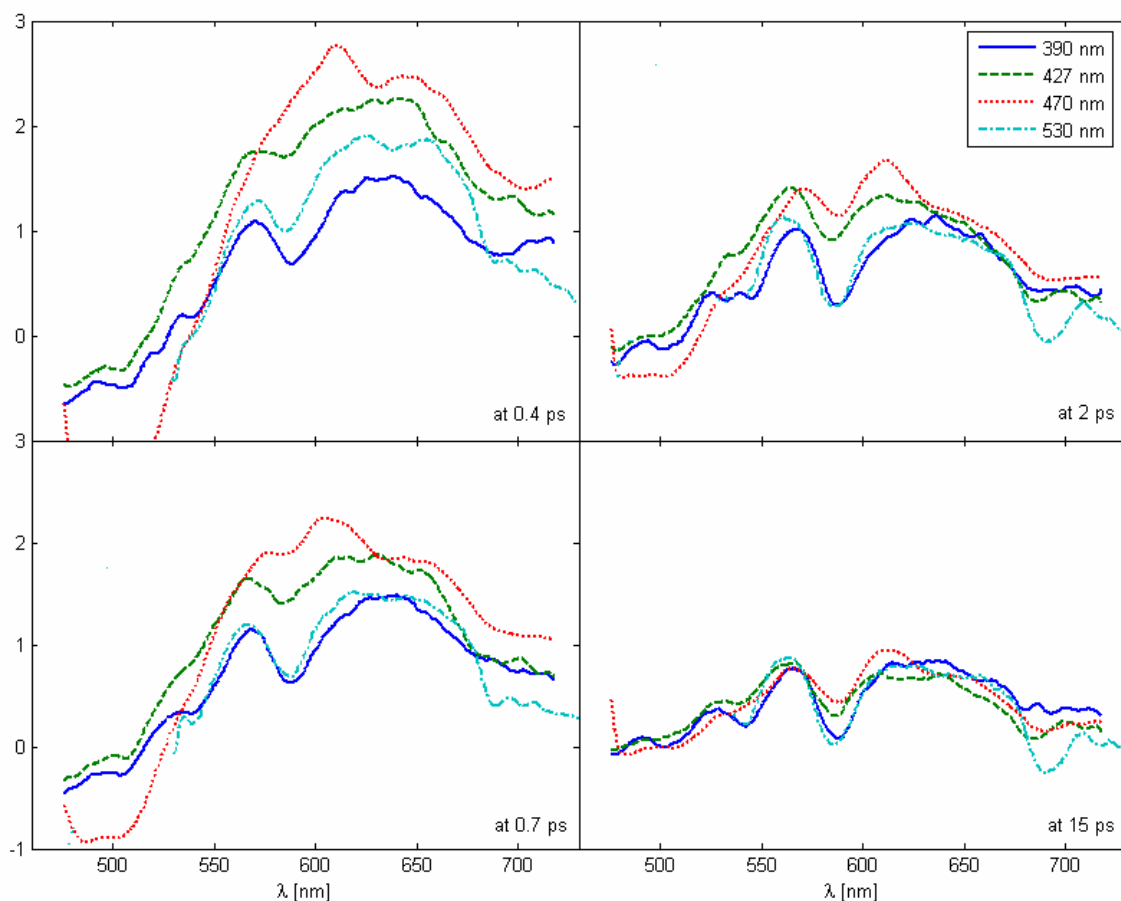

Fig.: 17 Transient absorption spectra of PCP reconstituted with Bchl-a in relative units recorded for different excitation wavelengths (390, 427, 470 and 530 nm). Region below 540 nm is omitted in the case of 530 nm excitation because of the strong pump scattering into the signal.

We can see that the data obtained after 470 nm excitation differs from the others in many ways, especially at very short delay times after excitation. Experiments were performed only once, implying an explanation based on possible experimental error, but on the other hand all experiments were performed on the same sample and under identical experimental conditions. This suggests that these differences may have a natural origin. The most striking difference is the peak at 607 nm that appears exclusively in the data recorded with 470 nm excitation. Although a small error can be caused by the inaccurately treated chirp compensation (2.), it cannot explain the 607 nm peak, because the errors related to the chirp compensation would be limited to the very early times after excitation. Yet, the 607 nm peak is clearly visible even at later delay times. At this moment, there is no plausible explanation for the appearance of the 607 nm peak in the 470 nm excitation data, and new experiments are needed to eliminate a possibility of an artefact.

In all spectra we can clearly distinguish a valley centred at 586 nm due to Bchl-a Q_x band bleaching superimposed at the broad excited state absorption of peridinins. Since we have excluded direct excitation of Bchl-a, the presence of this peak is a clear sign of energy transfer from the peridinins to Bchl-a. A more intensive bleaching of Bchl-a band at 585 nm is observed after 390 and 530 nm excitations (Fig.: 17). After 530 nm excitation this result could be explained by a favourable overlap between the S_2 emission of the red peridinins and the Q_x band of Bchl-a located at 580 nm. This situation promotes efficient S_2 to Q_x energy transfer explaining the presence of the Q_x bleaching at the very early times after excitation. Because the bleaching increases further with the increasing time delay, it implies that the red shifted peridinins excited at 530 nm likely transfer energy to the Bchl-a most efficiently (their S_1/ICT energy is likely also closer to the Bchl-a levels than for other peridinins in PCP).

On the other hand, the intensive bleaching obtained after excitation at 390 nm calls for more elaborate explanation. Firstly, the 390 nm excitation pulse could partially excite Bchl-a directly (spectroscopic properties of Bchl-a depends slightly on the environment, and the Soret band usually exhibits two smaller peaks with the higher at 358 and the smaller one centred almost exactly at 390 nm in diethyl ether [22]). This logically would cause bleaching immediately after excitation. An alternative explanation is a fast energy transfer from the blue peridinins to the red peridinins via S_2-S_2 energy transfer predicted in some earlier works [27]. Comparing the data presented here, the most favourable explanation would be the S_2-S_2 coupling between blue and red peridinins,

because both blue (390 nm) and red (530 nm) excitations produces significant Q_x bleaching at the very early times after excitation. Yet another explanation could be a transfer of energy from the blue shifted peridinin directly to the Soret band of Bchl-a. This process can be mediated only by the S_2 state, because energy of the S_1/ICT state does not allow for such energy transfer pathway. Because the S_2 state mediated processes are on the verge of resolution of the used setup they may appear immediate. This finally makes the possible S_2-Soret energy transfer process indistinguishable from the direct excitation of Bchl-a. The hypothesis that there is no energy transfer between the blue peridinin and Soret band, and probably also no S_2-S_2 transfer between blue and red peridinins seems more probable, but a better time resolution is necessary for the definitive solution of the problem.
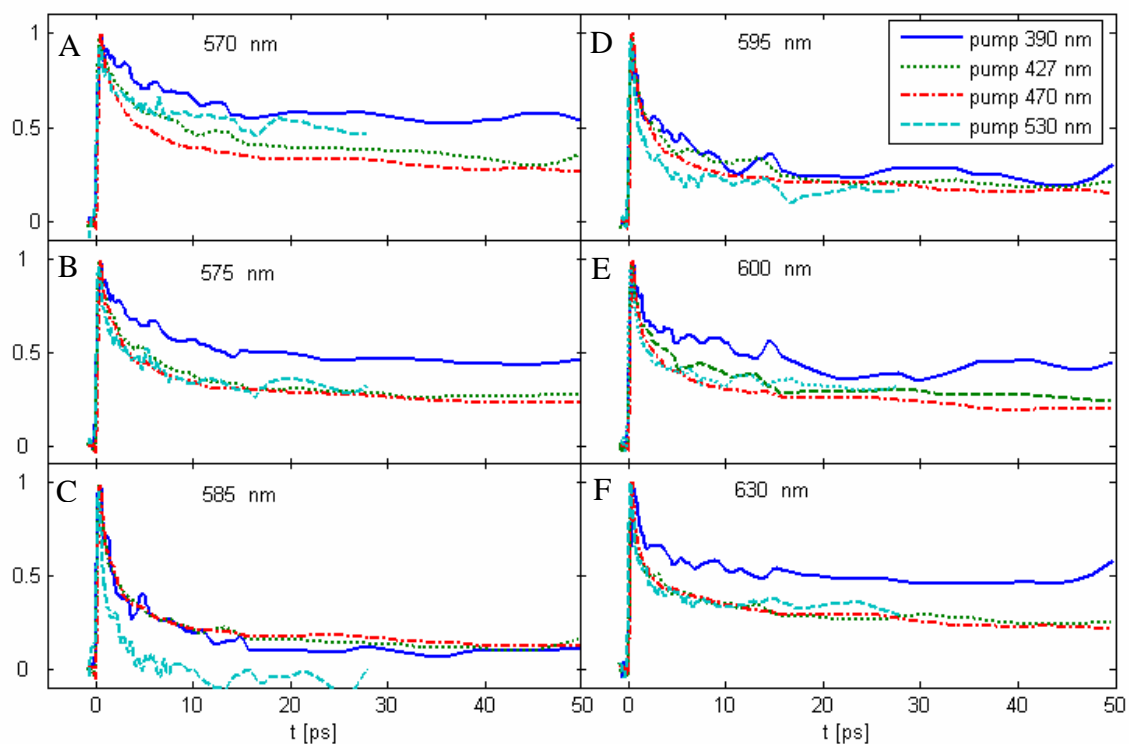

Fig.: 18 Kinetics recorded for the PCP reconstituted with Bchl-a at selected probing wavelengths (570, 575, 585, 595, 600 and 630 nm) and their dependence on excitation wavelength.

Additional information can be obtained by comparing kinetics recorded at selected wavelengths. Kinetics at selected wavelengths are depicted in Fig. 18.

The first thing which we can conclude from these kinetics is a confirmation that both 390 nm and 530 nm pump excite different pigments or at least the same pigments in a different proportion. On the other hand, because the kinetics obtained after excitation at 427 and 470 nm always appear similar (Fig. 18), it most likely means that the same pigments are excited at these wavelengths. Because the region 578-589 nm (Fig. 18 C) corresponds well to the Bchl-a Q_x bleaching peak, this region reflects best the peridinin-Bchl-a transfer. The result that the 530 nm excitation causes the most intensive bleaching of Bchl-a (similar to preceding qualitative analysis of transient spectra) implies that this excitation hits the peridinins that relay energy to Bchl-a most efficiently, and that these efficient peridinins are most likely associated with the red part of the PCP absorption spectrum.

Kinetics also confirm the assumption that there must be some direct excitation of Bchl-a after 390 nm excitation, but slower transfer of excitation to Bchl-a also occurs after 390 nm excitation as demonstrated by the decay of the S_1/ICT signal in the whole spectral region. Further insight into the complicated excited state dynamics can be obtained by application of global fitting analysis [20] (3.2.2).

3.2.2 Global fitting analysis

All recorded datasets were fitted with an assumption that there exists at least four independent excited state species chained successively together by three time constants (A→B→C→D) (2.3). Energy transfer schemes and associated time constants could be established by comparing the spectral profiles of the fitted components, usually termed evolution associated difference spectra (EADS), with known excited-state spectra. A weak point of this particular analysis is the presumed sequential scheme. If there is a branching in energy transfer pathways, this sequential model creates components consisting of a mixture of states and the time constant is set somewhere in the middle of both successive processes. This situation clearly occurs in PCP, because it is a well-established fact that the peridinin S_2 decays in a branched pathway; it transfers energy to chlorophyll and decays into the S_1/ICT state [3] Despite this limitation, fitting to the sequential model is very useful to visualize excited state dynamics [20]. It is usually possible to recognize a mixture of two states in the fitted components and to set the branching point of the relaxation and energy transfer pathways.

The first spectral component is associated mostly with the S_2 excited state absorption, bleaching and stimulated emission [2] of peridinin, but with a pulse width around 130 fs extracting the pure S_2 spectrum is beyond the time resolution of the measurement (lifetime of the peridinin S_2 state in solution was determined to be shorter than 100 fs, slightly dependent on polarity [2]). This causes that the first component mirrors a mixture of very fast processes blurred by the insufficient time resolution, and can not be easily interpreted. This explains why this component differs significantly among the individual datasets, while the other components display strong resemblance for the datasets measured with different excitation wavelengths.

The second component is attributed mostly to the peridinin S_1/ICT state spectrum. It contains peridinin ground state bleaching below 500 nm and a broad featureless band peaking around 640 nm that extends from 500 nm to the near-IR region that is characteristic of peridinin excited state absorption (1.3).

The third component resembles Bchl-a excited state absorption with characteristic bleaching of the Q_x band at 585 nm. On the other hand, the existence of a small amount of the S_1/ICT state in this component is recognized by a small, but evident bleaching signal below 500 nm. The mentioned S_1/ICT contribution could result from a presence of a peridinin that does not transfer energy to Bchl-a or does it significantly slower [21] (Fig.: 19).
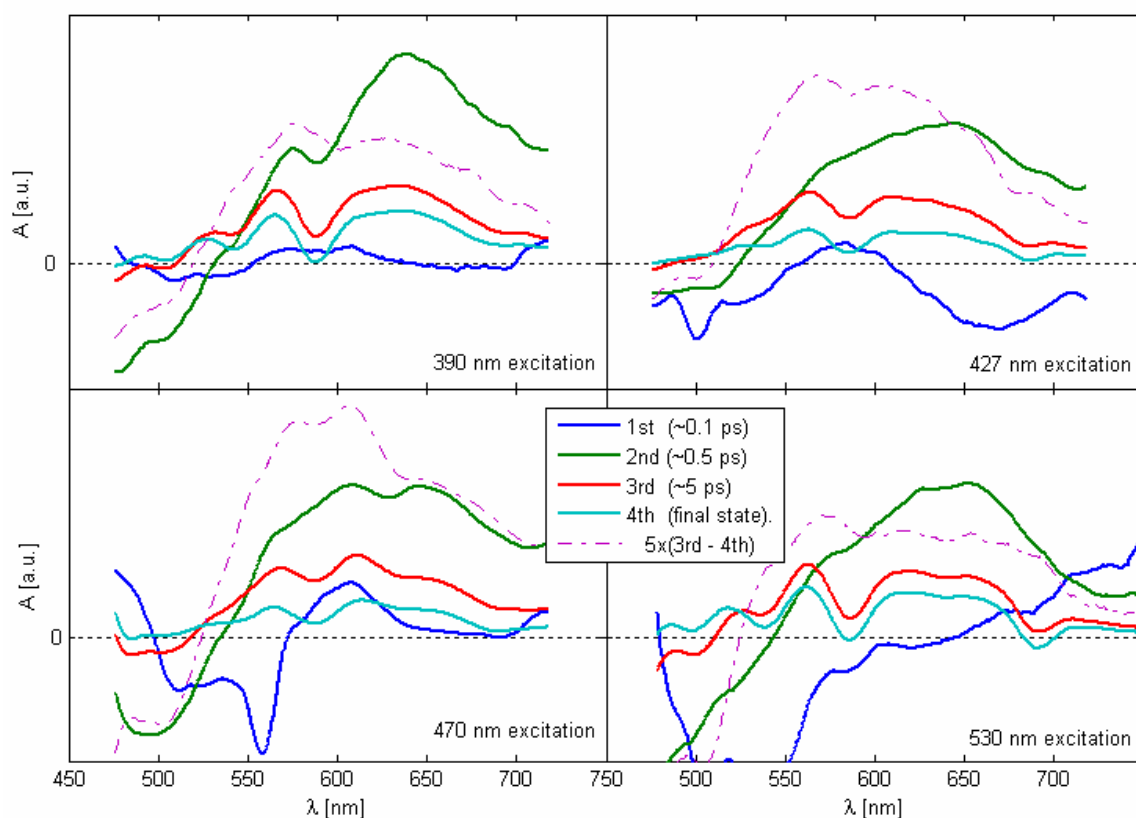
Fig.: 19 Evolution associated difference spectra (EADS) obtained by global fitting of the data measured after excitation of PCP substituted by Bchl-a at different wavelengths. The first component mostly describes the S_2 state of peridinin, the second is dominated by the S_1/ICT state of peridinin, the third represents a mixture of Bchl-a excited state absorption and the S_1/ICT of a slow-transferring-peridinin, the final, non-decaying component is the Bchl-a excited state absorption. The dash-dot line is obtained by subtraction of the 4th and 3rd components. The resulting difference spectrum is multiplied by 5 to make it comparable with other components, and it is assumed to represent the S_1/ICT spectrum of the slow-transferring-peridinin.

The fourth component consists of a pure Bchl-a excited state absorption. The reason is that it looks similar to the third component but it lacks the bleaching below 500 nm discussed above.

The spectral components obtained after 390 nm excitation show that the bleaching at 585 nm is clearly distinguishable in the second, and partially even in the first component of the fit. This suggests that both the direct excitation of Bchl-a (bleaching in the first component) and energy transfer from the peridinin S_2 state (bleaching in the second component) takes place. By the use of similar arguments, a small amount of the direct excitation of Bchl-a can be also distinguished from the first fitted component of the 530 nm excitation as a small bleaching at 585 nm. The difference between this case and the 390 nm excitation is the lack of an evident increase of the bleaching signal when

going from the first to the second component, indicating a very small or no contribution of the S_2 to Bchl-a energy transfer after 530 nm excitation. This is valid also for 425 and 470 nm excitation, so it is possible to conclude that the substantial peridinin to Bchl-a energy transfer via the S_2 state occurs only after 390 nm excitation.

The time constants associated to these components are summarized in Table 1:

Pump wavelength	τ_{1-2} (ps)	τ_{2-3} (ps)	τ_{3-4} (ps)
390 nm	<0.1 ps	0.56	5.3
427 nm	<0.1 ps	0.56	8.4
470 nm	<0.1 ps	0.48	6.2
530 nm	<0.1 ps	0.57	3.6

Table 1: Time constants associated with transitions between individual excited state species in the sequential model extracted from the global fitting of the data.

The time constants confirm the trend of slightly different results for the 470 nm excitation. If it is considered that at this wavelength the simultaneous excitation of all peridinins is most likely, and that excitation of Bchl-a is negligible, it can be expected that this particular excitation would result in the "most standard" excited state dynamics. From this point of view the possible explanation of the differences is that they are most likely related to artefacts.

The peridinin bleaching in the third spectral component, presumably related to a slowly- or non-transferring peridinin, is most distinguishable for 530 and 470 nm excitations. To clarify this surmise the difference spectra of the third component (assumed to be the mixture of Bchl-a and peridinin signal) and fourth component (assumed to be pure Bchl-a signal) were constructed. These difference spectra (DS) are depicted in Fig.: 18. Despite the fact that these DS differ from the second components (assumed to be the S_1/ICT spectrum of the peridinins) the DS resemble each other for all excitation wavelengths (except the discussed 470 nm excitation (3.2.1)). In contrast with the similarity on the shape of the DS, the absolute values of DS vary strongly with excitation wavelength. The fact that they are smaller for 390 and 530 nm excitations implies that the presumed non-transferring peridinin is neither the blue shifted nor the red shifted but some of the middle ones. A good candidate is the peridinin having its 0-0 transition at 520 nm (1.3). The extracted spectrum of the non transferring peridinin

resembles the spectrum of the peridinin S_1/ICT state obtained in a less polar environment. If we look at the time constants of the last evolution step (the 3rd to 4th EADS), we can see a strong variability in contrast to the other time components that are almost identical for all excitations. It should be kept in mind that the presence of the non-transferring peridinin violates the assumed sequential scheme of excited-state processes, so the model creates a mixture of true excited states, leading to false time constants that are influenced by the proportion of the individual processes. Consequently, the longer lifetimes of the third component obtained for 427 and 470 nm excitations may indicate that the "slow peridinin" is preferentially excited at these wavelengths, in agreement with the assignment of this peridinin to one of the middle ones. However, other processes such as the energy transfer and equilibration between the two Bchl-a molecules residing in PCP that occur on a similar time scale [15] may also interfere with the peridinin decay.

3.3 Degradation of the PCP

Absorption spectra of the sample were recorded before and after each measurement to follow degradation processes in the sample. A relative degradation spectra (RDS) were obtained by:

$$RDS(\%) = 100 \cdot \frac{\left(Abs_{before} - Abs_{after}\right)}{Abs_{before}}$$

Resulting RDS are depicted together with the absorption spectrum of PCP taken before the time-resolved measurements in Fig. 20:
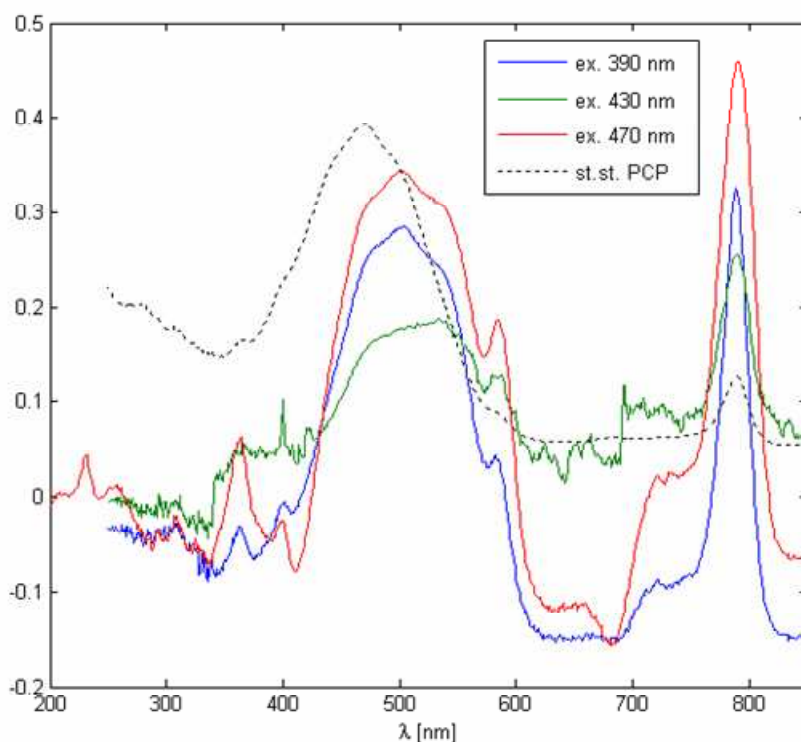
Fig.: 20 Relative degradation spectra (RDS) and absorption spectra of the PCP reconstituted by Bchl-a associated to individual time-resolved measurements differing only in the excitation wavelength.

RDS shows that the degradation of the samples was homogenous in a sense that a magnitude of the degradation in the peridinin and Bchl-a parts of the spectrum was similar and in the range of 2-4 ‰. The peaks responsible for the Bchl-a degradation are in a good agreement with the steady state spectra of PCP. This is especially valid for the main absorption peaks at 790 nm (Q_y band) and 585 nm (Q_x band). More questionable are the minor peaks at 364 and 400 nm. They match reasonably well with the Bchl-a Soret peaks at 358 and 390 nm (measured in diethyl ether [22]), but if these near UV peaks originated from degradation of the same Bchl-a as the 790 and 585 peaks, they should be much more intensive. Also the lack of the 358 nm peak in RDS after 430 nm excitation measurement implies that the origin of those peaks is likely not directly related to Bchl-a degradation. Sorting measurements according to the magnitude of the degradation we get the following sequence: 470 nm > 390 nm> 430 nm. It must be noted, however, that excitation intensities (in number of photons per pulse per cm^{-2}) were not identical in these three measurements, so this sequence does not necessarily reflect the influence of excitation wavelengths. But a closer inspection of the peaks and valleys at 364, 682, and 730 nm tells that their intensity increases by the same order.

This implies that these peaks are supposedly caused by products of degradation, such as formation of oxidized Bchl-a or other compounds that can arise from PCP pigments under intensive irradiation.

A very interesting feature of RDS is the fact that the peridinin peaks associated with degradation are significantly red shifted as compared to the PCP absorption spectrum. This means that degradation affects specifically the red peridinins in PCP. The position of the reddest peridinin band (usually belonging to the lowest 0-0 band of the S_0-S_2 transition) in RDS at 540 nm matches perfectly the expected 0-0 band of the red shifted peridinin in PCP [3]. Consequently, RDS allows for extraction of the absorption profile of the red peridinin that was in the structure identified as the peridinin 624/614 (Fig. 5) [6].
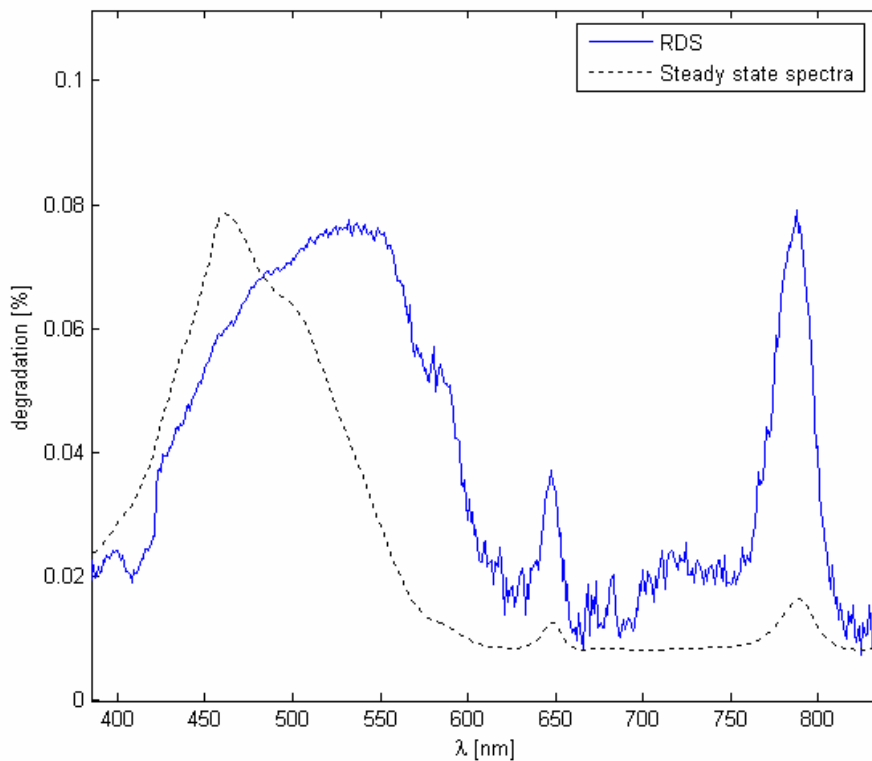

Fig.: 20 Relative degradation spectra of PCP reconstituted with a Bchl-a/Chl-b mixture together with the corresponding absorption spectrum.

Degradation of the PCP reconstituted with mixed chlorophyll sites was also measured. The RDS spectrum resembles the degradation of the Bchl-a reconstituted PCP and keeps the trend of degradation of the red shifted peridinins. Degradation of Bchl-a appears to be twice larger than that of the Chl-b confirming the result of Bchl-a/Chl-b affinity calculation predicting Bchl-a affinity being about half of the Chl-b (3.1).

4. Conclusions

The results presented in this thesis confirm the earlier results assigning the time constant of the main peridinin to Bchl-a energy transfer channel approximately to 0.5 ps [12] (3.2.2). For PCP reconstituted with mixed chlorophyll sites, the time constants of the peridinin to Bchl-a energy transfer was slightly faster, yielding a value of 0.4 ps (3.1.3). The results showed that, despite the large energy gap between the Q_y bands of Chl-b and Bchl-a, efficient energy transfer takes place between Chl-b and Bchl-a occupying the chlorophyll binding sites in PCP reconstituted with mixed chlorophyll sites (3.1.1). The measured energy transfer lifetime, 64 ps, has been successfully modelled by the Förster equation, confirming the earlier hypotheses that energy transfer between chlorophylls in PCP proceeds via the Förster mechanism (3.1.2).

Transient absorption experiments on PCP reconstituted with a single chlorophyll, Bchl-a, (3.2.1) supported by global fitting analysis (3.2.2) suggest that 390 nm pump excites predominantly the blue peridinins in PCP. These peridinins display a minor energy transfer channel to Bchl-a via the peridinin S_2 state, while no S_2 transfer was identified for other peridinins. Similarly, the 530 nm pump excites predominantly the red shifted peridinins that seem to transfer energy to Bchl-a most efficiently, but the results are not as convincing as in the case of 390 nm excitation. For both 390 and 530 nm excitation wavelengths, a direct excitation of Bchl-a takes place to a certain extent.

Global fitting analysis does not bring any evidence of energy transfer between peridinins, but implies the existence of a slow-transferring peridinin [12]. The best candidate is the peridinin having the 0-0 transition located around 520 nm. Approximate S_1/ICT spectrum of this peridinin was extracted from the fitted components (Fig.: 19).

Analysis of photoinduced degradation (3.3) does not reveal any qualitative dependence of the sample degradation on the excitation wavelength. Instead, regardless of the excitation wavelengths (390, 427, 470 nm) the peridinins having the most red shifted absorption together with chlorophylls are predominantly bleached, implying their possible photo-protective function. Some minor, unexplained features appear in the relative degradation spectra, probably the results of photochemical reactions generated by prolonged excitation of the PCP samples. The relative degradation spectra together with theoretical analysis of absorption spectra of the PCP complexes reconstituted with

mixed chlorophyll sites suggest that binding affinity of Bchl-a to PCP appoprotein is about half of that of Chl-b.

5. References

[1] Frank H. A., Cogdell R. J., Phototochem. Photobiol. 63 (1996) 257-264.

[2] Polivka T., Sundström V., Chem. Rev. 104 (2004) 2021-2071.

[3] Polivka T., Hiller R. G., Frank H. A., Arch. Biochem. Biophys. 458 (2007) 111-120.

[4] Macpherson A. N., Hiller R. G., in Green R.G., Parson W.W. (Eds.) Light-Harvesting Antennas in Photosynthesis, Dordrecht, The Netherlands, (2003).

[5] Hofmann E., Wrench P., Sharples F. P. Hiller R. G. Welte W., Diederichs K., Science. 272 (1996) 1788-1791.

[6] van Stokkum I.H.M. et al., Chem. Phys. (2008), doi:10.1016/j.chem. phys. (2008).

[7] Kleima F. J., Wendling M., Hofmann E., Peterman E. J. G., van Grondelle R., van Amerongen H., Biochemistry. 39 (2000) 5184-5195.

[8] Carbonera D., Giacometti G., Segre U., Hoffman E., Hiller R.G., J. Phys. Chem. B 103 (1999) 6349-6356.

[9] Papagiannakis E., Vengris M., Larsen D.S., van Stokkum I. H. M., Hiller R.G., van Grondelle R., J. Phys. Chem. B 110 (2006) 512-521.

[10] Ilagan R.P., Shima S., Melkozernov A., Lin S., Blankenship R. E., Sharples F. P., Hiller R.G., Birge R. R., Frank H. A., Biochemistry. 43 (2004) 1478-1487.

[11] Miller D. J., Catmull J., Puskeiler R., Tweedale H., Sharples F. P., Hiller R. G., Photosynth. Res. 86 (2005) 229-240.

[12] Polivka T., Pascher T., Sundström V., Hiller R. G., Photosynth. Res. 86 (2005) 217-227.

[13] Polivka T., Pascher T., Hiller R.G., Biophys. J. 94 (2008) 3198-3207.

[14] Scholes G. D., Annu. Rev. Phys. Chem. 54 (2003) 57-87.

[15] Kleima F. J., Hofmann E., Gobets B., van Stokkum I. H. M., van Grondelle R., Diederichs K., van Amerongen H. Biophys. J. 78 (2000) 344–353.

[16] Damjanovic A., Ritz T., Schulten K., Biophys. J. 79 (2000) 1695-1705.

[17] Frank H. A., Bautista J. A., Josue J., Pendon Z., Hiller R. G., Sharples F. P., Gosztola D., Wasielewski M. R. J. Phys. Chem., B. 104 (2000) 4569.

[18] Zigmantas D., Hiller R. G., Frank H. A., Sundström V., Polivka T., Phys. Chem. Chem. Phys. 6 (2004) 3009-3016.

[19] Zigmantas D., Hiller R. G., Polivka T.., Sundström V., Proc. Natl. Acad. Sci. USA 99 (2002) 16760-16765.

[20]. van Stokkum I. H. M, Larsen D. S., van Grondelle R., Biochim. Biophys. Acta 1657 (2004) 82-104

[21] Krueger B. P., Lampoura S. S., van Stokkum I. H. M, Papagiannakis E. Salverda J. M. Gradinaru C. C. Rutkauskas D., Hiller R. G., van Grondelle R., Biophys. J. 80 (2001) 2843-2855.

[22] van Amerongen H., Valkunas L., van Grondelle R., Photosynthetic Excitons (2000) World Scientific Publishing Co. Pte. Ltd.

[23] Mimuro M., Nagashima M., Takaishi S., Nishimura Y., Yamazaki I., Katoh T., Biochim. Biophys. Acta 217 (1992) 1098.

[24] Zigmantas D., Polivka T., Hiller R. G., Yartsev A., Sundström V., J. Phys. Chem. A 105 (2001) 10296.

[25] Zigmantas D., Hiller R.G. Yartsev A., Sundström V., Polivka T., J. Phys. Chem. B 107 (2003) 5339.

[26] Kukura P., McCamant D. W., Mathies R. A., Annu. Rev. Phys. Chem. 58 (2007) 461

[27] Ilagan R. P., Koscielecki J. F., Hiller R. G., Sharples F. P., Gibson G. N., Birge R. R., Frank H. A., Biochemistry 45 (2006) 14052.

[28] Allen L., Eberly J. H., Optical resonance and two-level atoms, Dover Publication, Inc., New York (1975) ISBN 0-486-65533-4.